2006: The Journal of Astronomical Data 12, 3.

An overview of the photometric events, trends and brightenings of η Carinae

A. M. van Genderen[1], C. Sterken[2,*], W. H. Allen[3] and W. S. G. Walker[4]

(1) Leiden University Observatory, Postbus 9513, NL-2300RA Leiden, The Netherlands
(2) Vrije Universiteit Brussel, Pleinlaan 2, 1050 Brussels, Belgium
(3) Alvine Estate, Vintage Lane, RD 3, Blenheim, New Zealand
(4) 272 Heath Road, Awanui RD 1, New Zealand 0451

Received 27 October 2006, accepted 13 December 2006

Abstract

Using new and archived ground-based optical and near-infrared photometry (covering more than three decades) and space-based (HST) narrow-band photometry, we document the morphological character of optical and near-infrared photometric features at seven periastron passages of η Carinae, of the secular brightening 1952–1998, of the brightening episodes after the 1997.9 and 2003.5 events, and of two types of UV oscillations, with the purpose of getting some insight in the causes of these variations.

The optical peaks could be the climax of the expansion phase of the primary due to tidal effects. The dips can be explained by obscuration of the secondary's circumstellar structure by the (polar) wind of the primary. The wavelength dependency of the rates of the slow secular brightening (1952–1997.9), and of the fast brightenings of the central star and Homunculus after the 1997.9 and 2003.5 events are investigated. The brightenings can be interpreted as an extinction decrease with an extinction law $R \sim 5$.

The primary's luminosity and mass-loss rate were likely stable over the last 35 yr. The long-term UV oscillations are interpreted as revolution-modulated H-emission variation in the equatorial plane, whereas the short-term UV oscillations are due to stellar pulsations.

Keywords: technique: photometric – stars: η Carinae – supergiants – oscillations

*Research Director, Belgian Fund for Scientific Research (FWO).

1 Introduction

A hot companion to η Car was indirectly detected in the far-UV by Iping et al. (2005). A number of 5.54-year periodic features in various spectral regions were already explained by the presence of a companion, see, for example, Damineli (1996) and Corcoran (2003). Some models of the Homunculus morphology also require a binary configuration (Soker 2005). The great variety of observations have led to diverse interpretations and orbital configurations (e.g. Davidson 1999; Ishibashi et al. 1999; Corcoran et al. 2001; Pittard & Corcoran 2002; Smith et al. 2004; Steiner & Damineli 2004; Falceta-Gonçalves et al. 2005; Akashi et al. 2006).

All ground-based optical photometry is dominated by the Homunculus, and the central star is about 2–3 magnitudes fainter than the integrated circumstellar structure. As such, η Car is to be regarded as the most difficult stellar object to photometrically monitor (for a detailed discussion, see Sterken et al. 2001a). But the general opinion that large aperture photometry is unreliable for studying the variability of the central star is unfounded: a comparison of HST photometry of the isolated core with simultaneous ground-based photometry shows that the Homunculus mimics the *intrinsic* light variations of the core quite well (van Genderen & Sterken 2004, 2005, see also Sect. 5.7).

To prepare the ground for ground-based monitoring campaigns at the upcoming periastron passage in 2009.0, we present an overview and a discussion of the optical and NIR behaviour of η Car during each of seven periastron passages that occurred during the last four decades. We confine our discussion to a time interval of approximately one year centered on each periastron passage.

2 Terminology

Each periastron passage[1] (PP) is preceded by a rising branch of the light curve which leads to a light peak ($0\overset{m}{.}1$–$0\overset{m}{.}2$) in the optical and near-infrared (NIR). The rising starts a couple of months before the PP. The steepest part of the optical light peak was called the *flare-like event* by van Genderen et al. (2003a). But it now becomes obvious that this brightening has no connection with a flare-like process: the peak is always followed by a steep decline ($0\overset{m}{.}1$–$0\overset{m}{.}2$), rather suggesting an obscuration process. After the decline a slower recovery occurs until a maximum is reached: the *egress-maximum*. We will refer to the enclosed (asymmetric) depression as the *dip*. This sequence of photometric features will be called the *photometric event* (the *optical event* or the *NIR event*). We also discuss the wavelength dependency of the rates of the secular brightening of two fast brightening episodes observed after the 1997.9 and 2003.5 events, called the *post-egress brightenings*, and of the fast brightening of the central star from 1998 to 2000.

The first indication of a peculiar light peak in the optical close to the time of periastron occurred at the end of 1997. The $0\overset{m}{.}1$ peak in the Geneva passbands seemed to last about two months, but due to poor sampling, no detailed morphology was visible (van Genderen et al. 1999). Strömgren photometry became eventually available with a better coverage

[1] Periastron passage is defined as the timing of the peak of the H II intensity, see Steiner & Damineli (2004).

(Sterken et al. 1999a,b; van Genderen et al. 2003a,b). An eye-catching fact in both data sets was that the peak amplitude in the Balmer continuum bands ([U], u), was 1.5 times larger than in the other bands, with a dip depth that was even twice as large. This supported the assumption that the feature was of non-stellar origin.

The better coverage of the 2003.5 event showed a strong increase of the rate of brightening 1.5 month ahead of the PP. We now believe that also the less steep part some months ahead of this feature belongs to this phenomenon, see e.g. the V light curve in Fig. 1.

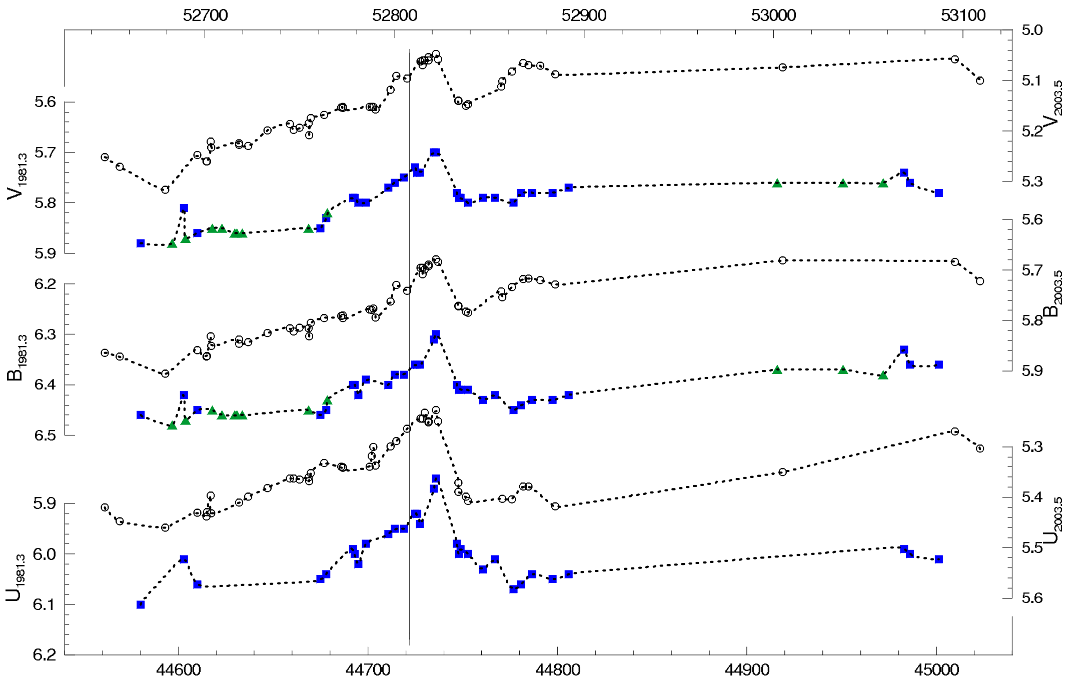

Figure 1: UBV light curves of the events of 2003.5 (magnitudes on the right, JD axis at the top) and 1981.3 (magnitude scale on the left, JD axis at the bottom). Vertical line: PPs; ○: 2003.5, Allen et al. (2005); ■: 1981.3, data from Walker (see Appendix); ▲: 1981.3, van Genderen & Thé (1984). The dotted lines are spline fits.

3 Description of the optical features

3.1 The 2003.5 and 1981.3 optical events

The best observed optical events are those of 2003.5: in $UBVRI$ (van Genderen et al. 2003b; Allen et al. 2005) and in $BVRI$ (Lajús et al. 2003), and of 1981.3 in UBV (data in Appendix). The PP of 2003.5 is assumed at JD 2452808, i.e. 17 June 2003 (Steiner & Damineli 2004). Fig. 1 shows the V, B and U light curves of 2003.5 and 1981.3. The curves cover from about half a year before the peak, until half a year after maximum light. The overall similarity of the peaks and declines is striking, especially in V and B, but less so in U

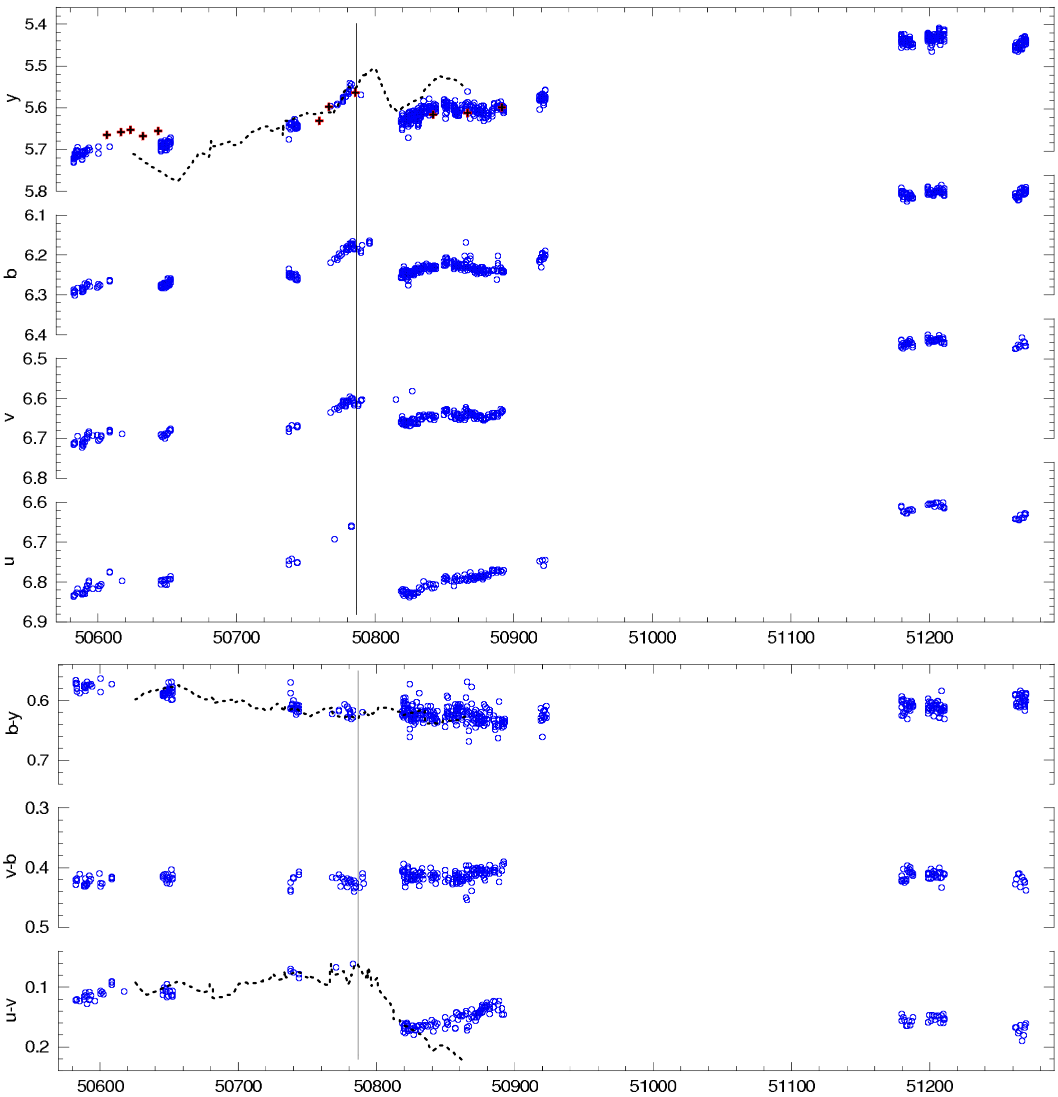

Figure 2: *uvby* light curves of the 1997.9 event including the fast part of the post-egress brightening (based on data from Sterken et al. 1999b). +: Geneva *V* (van Genderen et al. 1999). Vertical line: PP. The dashed lines are spline fits to the 2003.5 *uvby* magnitudes fitted by matching the ascending branches and times of PP. Colour scales are 1.5× the *y* scale (data from Sterken et al. 1999b).

because of the disturbing short-term UV oscillation (Sect. 5.8.2). The only outspoken difference between both sets of light curves is that the 1981.3 event shows extremely shallow dips, without pronounced egress and egress-maximum. Note that the 2003.5 HST broad and narrow-band observations in *V* and the narrow-band observations in the UV of the isolated central region (Martin & Koppelman 2004) seem to be imitated by the Homunculus very well.

So far, no period was ever based on optical photometry alone. By matching the ascending branches of the two peaks, we obtain $P = 2021\overset{d}{.}5 \pm 0\overset{d}{.}5$, which compares very well with the period for the spectroscopic events: $2022\overset{d}{.}1$ (Steiner & Damineli 2004). Both are compatible with the periods derived from the NIR photometry (2023 ± 3 d, Whitelock et al. 2004), and the period derived from the X-ray light curves (2024 ± 2 d, Corcoran 2005). Throughout this paper we use this photometric period together with the 2003.5 PP as zeropoint (JD 2452808, Steiner & Damineli 2004).

3.2 The 1997.9 optical event

The 1997.9 optical event was well covered in the *uvby* system (Sterken et al. 1999b) with only a few observations in the Geneva system (van Genderen et al. 1999). Fig. 2 shows the *uvby* light and colour curves together with the Geneva data points in V (shifted vertically to match the y light curve). The resemblance of the 2003.5 and 1997.9 curves until 75 days after the PP is quite good. The steep $u-v$ decline right after the PP is caused by the decline of the short-term UV oscillation, which occurred at this moment (Sect. 5.8.2 and Fig. 14).

The ascending branch started closer to the PP than the previously discussed ones (around JD 245 0725), see also the NIR light curves (Fig. 5), and has a lower amplitude. The onset of the extreme 1998–2000 brightening is obvious. The $b-y$ curve shows a reddening trend continuing up to a few months after the PP, and is similar to that of the 2003.5 event. $v-b$ shows a red minimum at the PP, and $u-v$ shows – like $U-B$ during the 2003.5 event (Figs. 1 and 3) – a steep and short lasting reddening trend ($0\overset{m}{.}1$) right after the PP (see above), followed by a blueing trend. The blueing trend for the 2003.5 event occurs a few months later (see Fig. 3).

3.3 The 1975.8 and 1986.8 optical events

The optical events of 1975.8 and 1986.8 have been sampled at a much lower frequency. Fig. 3 shows the V, $B-V$ and $U-B$ curves. V and $V-B$ are combinations of UBV and $VBLUW$ translated to the V and $B-V$ scale of the UBV system and subsequently shifted to match the data in the Johnson system. The 2003.5 light and colour curves of Fig. 2 are shown and matched by fitting the ascending branches of the light peaks and times of PP.

The 1975.8 event has one data point at the time of the expected dip, and the 1986.8 peak, decline and dip are badly sampled as well.

The distribution of the 1975.8 and 1986.8 data points in the $B-V$ diagrams reveals the trend observed for the normal curves: a slow reddening before the PP until some time thereafter, and subsequently a slow blueing lasting a couple of months, quite in accord with the expected behaviour.

One should realize that the V and $B-V$ curves during the events may be slightly influenced by the underlying S Dor-type variations, which usually have a much longer time scale (Sect. 5.3). It is obvious that $U-B$ suffers from the short-term UV oscillation (Sect. 5.8.2), for example, compare the excessive blueing in $U-B$ after the 1986.8 PP, with the one of 2003.5 which shows a reddening trend. Such a trend is also present in the 1981.3 $U-B$ curve (not shown).

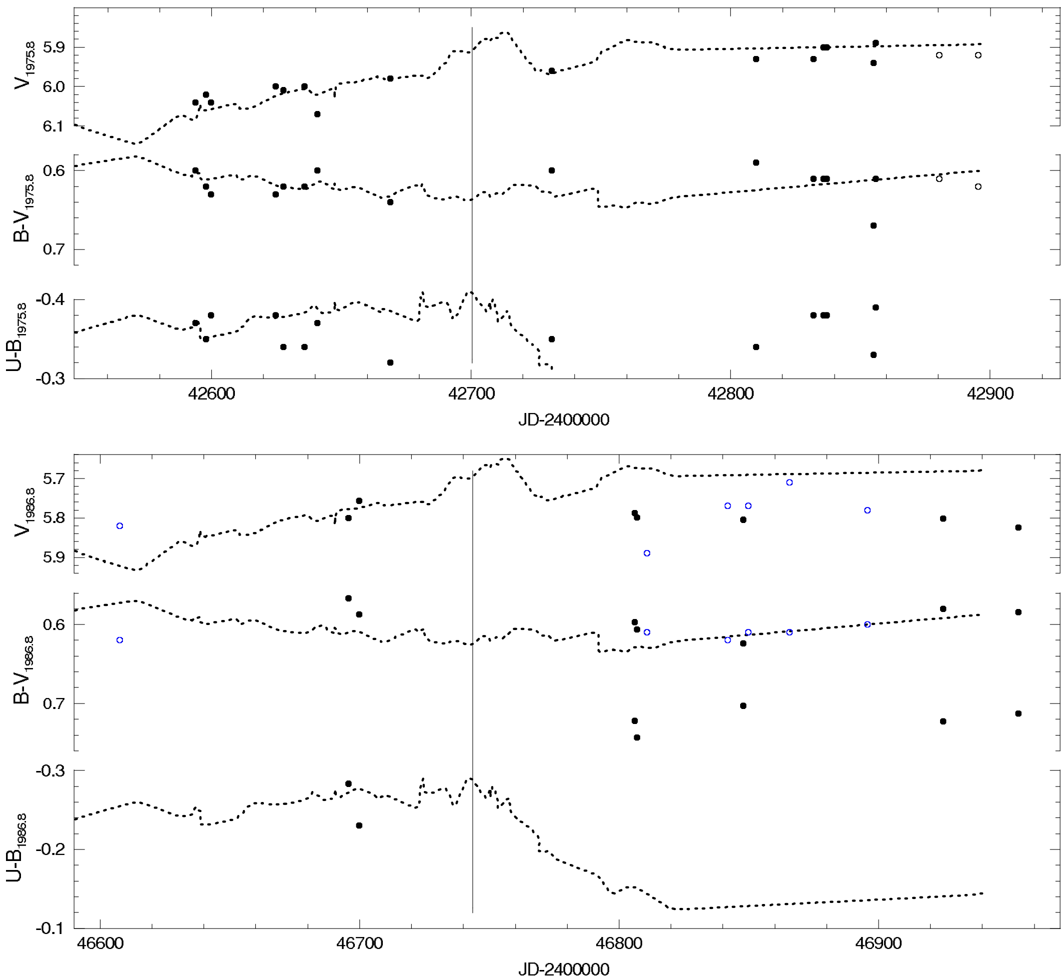

Figure 3: The light curves of the optical events of 1975.8 and 1986.8. Vertical line: PP. Colour scales are twice the magnitude scale. The dotted lines are the 2003.5 spline fits which match the ascending branches and times of PP. • 1975.8: Walker (see Appendix); ∘ 1975.8: van Genderen & Thé (1984). • 1986.8: Walker (see Appendix); ∘ 1986.8: van Genderen et al. (1994).

It can be concluded that the event of 1975.8 was marked by an increase in brightness before the PP. The $B-V$ trend before and after the 1975.8 and 1986.8 events bear the signature of an optical event. Together with the 1986.8 dip and egress-maximum in the NIR, we safely can assume that both events were also distinguished by the usual optical features.

3.4 The 1992.4 optical event

During the 1992.4 PP a light peak ($\sim 0\overset{m}{.}1$ amplitude) was detected (van Genderen et al. 2003a). Although the photometric scatter was relatively large, the $B-V$ trend before and after the PP was similar to the ones previously discussed, but data supporting a decline, and an egress-maximum, are lacking.

3.5 The 1970.2 and earlier optical events

UBV observations made between 1963 and 1973 (Feinstein 1968, Feinstein & Marraco 1974) are marked by large gaps between small groups of observations, lasting 1–2 years. No information is available on the 1964.7 PP (JD 243 8657.5) because it was situated precisely in such a large gap in the time series. However, four observations were made two weeks after the 1970.2 PP (JD 244 0679.0), viz. between JD 244 0693 and JD 244 0696. These four data points are indeed brighter by about $0\overset{m}{.}1$ with respect to the mean slow rising trend exhibited by this data set due to the secular brightening, thus indicating that a peak was present.

3.6 Summary for the optical events

The appearance of a light peak (0–$0\overset{m}{.}2$) during the PPs seems to be a common phenomenon, lasting 1–4 months with a light maximum about two weeks after the PP. The earlier the onset of a rising branch preceding PP, the higher the amplitude. The maximum is followed by a steep decline ($0\overset{m}{.}05$–$0\overset{m}{.}15$) lasting two weeks, and by a shallow dip. The egress runs much slower and is sometimes hardly present, so that a true dip and an egress-maximum are missing. The moment of the decline as well as the minimum of the dip are much more phase-locked than the start of the peak.

General features from the start of the peak: $B-V$, $b-y$ show a slow reddening until 2–4 months after the PP ($0\overset{m}{.}05$–$0\overset{m}{.}1$) interrupted by a small blue bump, two weeks after the PP. $v-b$ displays a red dip at the PP, and $U-B$ shows no stable pattern due to the short cyclic UV oscillations. Thus, no strong discontinuities in the colours during peaks and dips, apart from $U-B$ and $u-v$, do occur.

4 The near-infrared events

4.1 Introduction

The NIR light and colour curves (*JHKL*) and the features during the PPs were discussed by Whitelock et al. (1994, 2004), Whitelock & Laney (1999) and Feast et al. (2001). Some of the particulars described here were already noted by these authors, but as we need for our purpose a more detailed picture of light and colour behaviour around the PPs in order to compare them with the optical data, we recapitulate some of these features.

4.2 The 2003.5 and 1981.3 NIR events

Fig. 4 shows the *JHKL* curves for the 2003.5 event overplotted with the individual data points of the 1981.3 event. Like in the optical, the 2003.5 curves are well sampled and show detailed humps and bumps (the dimple in the $J-L$ colour index right in the minimum of

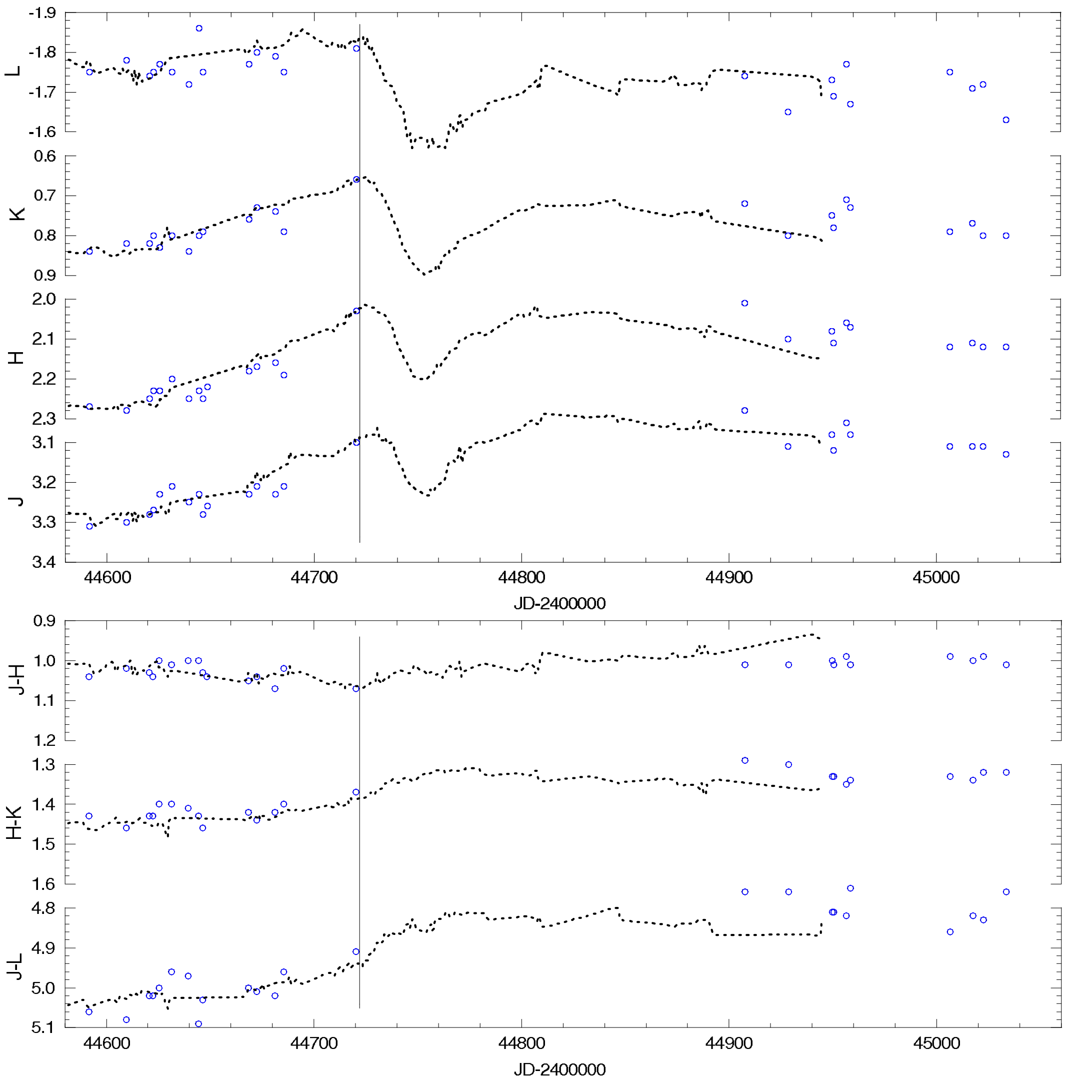

Figure 4: The $JHKL$ light and colour curves of the 1981.3 event (data from Whitelock et al. 1994, 2004). The superimposed dotted curves are the mean light curves of the 2003.5 event by matching the rising branches, the light maxima and the PPs. Vertical line: PPs.

the dip may be coincidential, but its occurrence at that moment is noteworthy). The 1981.3 curves are incomplete. The morphology of the NIR features is more wavelength dependent than in the optical. A large gap in the NIR time series after the 1981.3 PP occurs at the time of optical egress-maximum, but the high brightness about 200 days after the 1981.3 PP, even surpassing the post-egress brightening of 2003.5, is puzzling. The brightness declined thereafter in all NIR and optical channels by several $0\overset{m}{.}1$ until it reached the minimum level observed in 1984–1985 (Whitelock et al. 1994; van Genderen et al. 1994).

The 2003.5 NIR dips are deepest in L and shallowest in J (with respect to the peak maximum). Maximum light in L, K and H almost coincides with the PP, in J it occurs ten days later, whereas in the optical the maxima occurred about ten days later than in J, revealing a time delay progressive with wavelength. The X-ray radiation does not fit in this pattern (Corcoran 2005): maximum and even the start of the minimum are already passed by more than a month, by the time the optical reaches maximum light. This indicates that the source of the optical and NIR peaks is different from that of the X-ray radiation. The strength of the various high excitation lines and hydrogen lines starts increasing even before the time of X-ray minimum (e.g. Damineli 2004, priv. comm.; Davidson et al. 2005).

Noteworthy is: *i)* that the peak in L is very low compared to peaks in JHK, yet all start at the same time, and *ii)* that the minimum brightness of the LK dips is even lower than the brightness before the start of the peaks (by $0\overset{m}{.}2$ and $0\overset{m}{.}05$, respectively). The trends for the colours are almost similar for both events as far as can be judged from the scarce observations for the 1981.3 event.

4.3 The 1997.9, 1992.4, 1986.8 and 1975.8 events

Fig. 5 shows the 1997.9, 1992.4, and Fig. 6 (upper panel) the 1986.8 light curves. Because of the long-lasting post-egress brightening of 1997.9 (starting about 3 months after the dip) the light curves in Fig. 5 are shown until 450 days after the PP. It appears that the durations of the 1997.9 and 1992.4 peaks are shorter by 1–2 months than those of 2003.5 and 1981.3, and that instead of a peak, L shows a depression, see further. The amplitudes (with respect to the pre-peak brightness) seem to be related to the duration. Thus, the 1997.9 and 1992.4 JHK peak amplitudes are smaller. We suspect that this has a consequence for the height of the egress-maximum, which tends to be smaller as well.

The behaviour in L during the 1997.9 and 1992.4 peaks and at other wavelengths is even more peculiar than in 2003.5 and 1981.3. Apparently, the maximum is absent when JHK peaks are modest. Small peaks are also followed by dips with a brightness lower than the pre-peak brightness, not only in K and L, but also in H and J.

While the start (with respect to the PP) and the size of the peaks are more subject to variations from event to event, the start of the declines (with respect to the PP) and the depth of the dip (with respect to the maximum of the peak) are more phase-locked, just like in the optical.

Figs. 6 and 7 show for 1986.8 and 1997.9 the J light curve and the colour curves with the 2003.5 pattern overplotted. No observations were made at the 1976.8 PP, nevertheless, the signature of a passed event is clearly visible in, e.g., $J-L$ (Fig. 3 in Whitelock et al. 2004).

4.4 Summary for the NIR events

The variability in the NIR is generally stronger than in the optical, with almost equal durations of peaks. Like in the optical, the NIR peak amplitudes show a larger range than the dip amplitudes. The smaller the peaks in JHK, the more likely a peak in L is absent or even a depression occurs. Also, the dips tend to lie progressively deeper going from J to L, often the minimum brightness becomes fainter than the pre-peak brightness. This hardly occurred in the optical and is probably caused by the stronger concentration of the NIR to the core

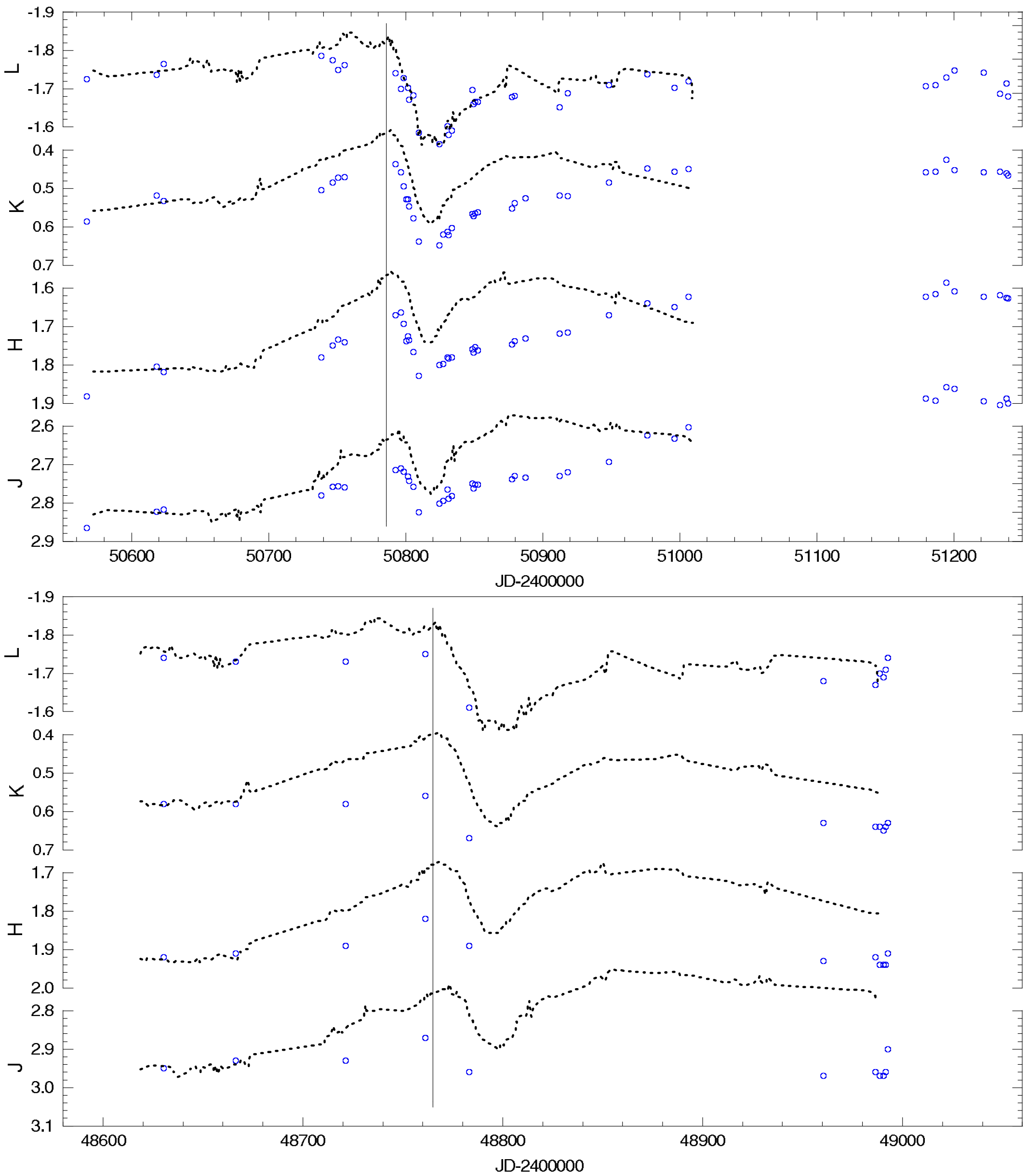

Figure 5: The *JHKL* light curves of the 1997.9 (including the fast part of the post-egress brightening) and 1992.4 events. The dotted curves are the 2003.5 spline fits of Fig. 4 matched by fitting the start of the peaks and the PPs (data from Feast et al. 2001 and Whitelock et al. 1994, respectively).

and the relative strong NIR radiation of the obscured source. It seems that events with small peaks have also less high egress-maxima and vice versa, see also Sect. 5.2.

The similarity of the colour trends during the events is surprising: the range of the colour changes varies from event to event. The general features from the onset of the peaks are:

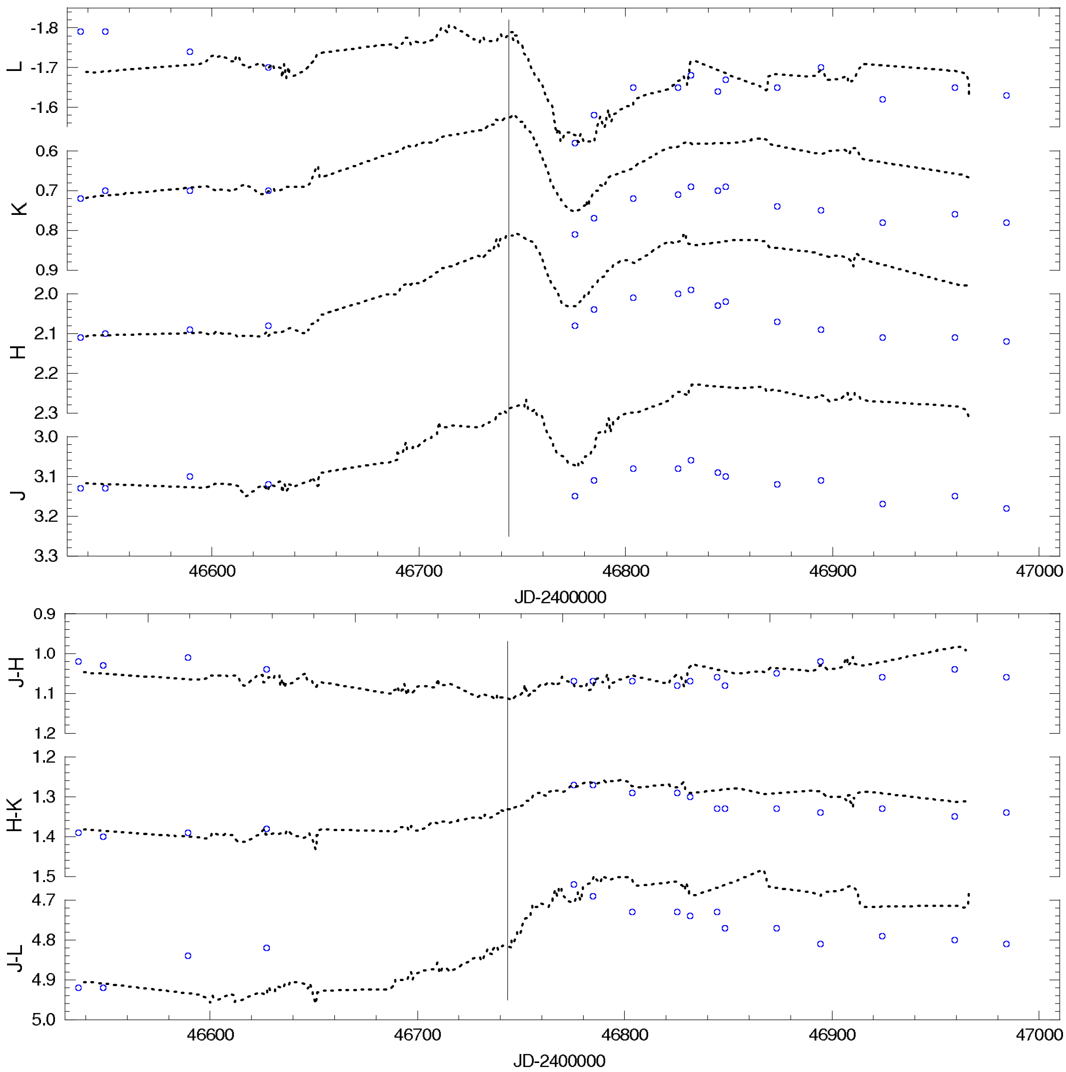

Figure 6: *JHKL* light and colour curves for the 1986.8 event (data from Whitelock et al. 1994). The dotted curves are the mean curves of the 2003.5 event and matched by fitting the start of the peaks and the PPs, and the colour curves are matched by fitting the colours during the minimum of the dip and the PPs. Vertical lines: PP.

1. $J-H$: a slow reddening ($0^{\rm m}\!.05$–$0^{\rm m}\!.1$) until maximum light, followed by a small blue bump three weeks later (note that this is almost coincident with the blue bump in $B-V$ and $b-y$) and a very slow blueing trend (the blueing rate three months after 1997.9 increases due to the abnormal post-egress brightening). The colour trend prior to the PPs indicates that the reddening trend begins about 400 days before the PP. It should be noted that in $b-y$ the reddening started about 300 days before the PP (Sterken et al. 2001a,b).

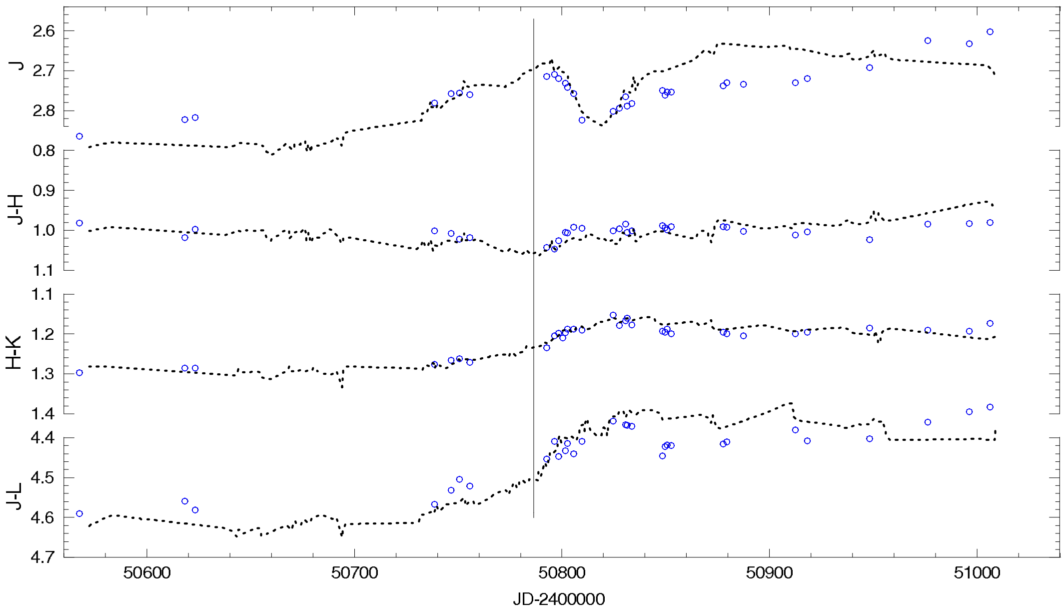

Figure 7: Light curve and colour curves for the 1997.9 event, however, the 2003.5 curves (dotted) are matched by fitting the light maxima of the peaks and the PPs (data from Feast et al. 1994). Vertical line: PP.

2. $H-K$: a slow blueing starts from the beginning of the peak until about a month after the PP ($0\overset{m}{.}1$–$0\overset{m}{.}15$), after which a slow reddening begins. It appears that the colour does not show a systematic trend from about 400 d prior to the PP.

3. $J-L$: the same as for $H-K$, but ranges are a factor two larger.

5 Discussion

5.1 The strong changes in $H-K$ and $J-L$

The PP is obviously an episode with great changes for the K and L radiating source, considering the strong changes in the $H-K$ and $J-L$ curves. K and L magnitudes decrease with respect to H and J, respectively, and the decrease starts a couple of months before the PP, and lasts a year or more after the PP. Whitelock et al. (2004) reject an orbital cycle of grain growth and destruction, although a dominant contribution of warm dust is suspected. Van Boekel et al. (2003) conclude that at 2.39 μm ($\sim K$ band), most of the emission should come from the ionized stellar wind and not from warm dust. Falceta-Gonçalves et al. (2005), on the other hand, show that conditions in their model are favourable for grain formation and growth during a short time around the PP. It appears that dust formation in a wind collision is fundamental to many models from cool to hot stars (see Soker 2005a). Continuous dust formation in the wind of η Car is advocated by various authors: e.g. Viotti et al. (1998), Smith et al. (2003a), Soker (2005a). Anyway, a deficit of K and L radiation is created during the close encounter since $H-K$ and $J-L$ become conspiciously bluer. It subsequently takes the K and L radiating material a year or more (Fig. 3 in Whitelock et al. 2004) to stabilise again. The way in which the equilibrium is reached is for each orbital cycle more or less the same with respect to morphology and the smoothness of the colour trends.

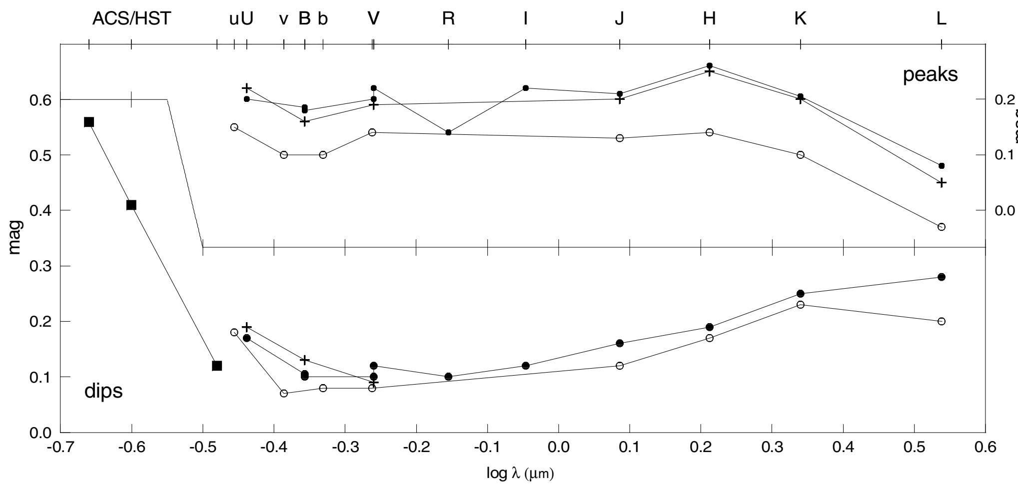

Figure 8: The wavelength dependency of peak heights and dip depths in magnitudes, upper and lower panel, respectively. •: 2003.5 event, *UBVR*, *BVRI* (Lajús et al. 2005) and *JHKL*. ■: 2003.5 event, ACS/HST narrow band photometry of the isolated central star (Martin & Koppelman 2004). ○: 1997.9 event, *uvby*, *JHKL*. +: 1981.3 event, *UBV*, *JHKL*.

5.2 The characteristics of peaks, dips and egress-maxima

The appearance of a light peak, a dip and a subsequent brightening to an egress-maximum in the spectral range 0.35–3.45 μm during a PP, is a common pattern during the photometric event.

Fig. 8 (upper part) shows for three well-covered events how the peak amplitude (i.e., the magnitude difference between the onset of the light peak and the maximum) depends on wavelength. The shape of the trends is not a strong function of wavelength, and the amplitudes are slightly larger in JHK than in the optical, and smallest in L. Positive amplitudes stand for a peak, negative amplitudes are noted when a depression in L is present. The fact that the 2003.5 R peak stands out because of its smaller size (by 30%), must be due to the influence of the Hα emission line which becomes weaker near periastron (Damineli et al. 1998), thus suppressing the growth of the peak in R.

The lower part of Fig. 8 shows the amplitudes of the dips (i.e., the magnitude difference between the maximum of the light peak and the minimum of the dip) as a function of wavelength for the same three events (though no red and NIR data are available for 1981.3). Again, the shape of the trends is very stable, but the wavelength dependency is stronger than for the peaks: in the NIR, especially in HKL, the dips are largest. The trends rise from the blue to the UV. Now the R amplitude fits in the sequence, the obscured body is apparently not the main contributor to the Hα radiation, otherwise the dip would have been much deeper than in the adjacent bands. Minimum brightness of the dips coincides with the minimum of the Hα emission line, but its recovery takes much more time than its decline (Davidson et al. 2005). The center of the X-ray minimum occurs almost two weeks later, see the X-ray light curve of Corcoran (2005).

Martin & Koppelman's (2004) analysis of the HST observations of the isolated core in 2003.5 shows that the increasing depth of the dips in the UV at 330 μm, 250 μm and 220 μm is mainly caused by a weakening of the FII forest of emission lines, mainly originating in the extended atmosphere of the primary (Gull & Ishibashi 2001). These dips are also plotted in the lower panel and fit more or less the UV trend shown by the Homunculus.

Peaks and dips are hardly traceable in the colour curves. Peak amplitudes and dip depths are not correlated. As a consequence, the question arises whether the egress-maximum showing a fading after a couple of weeks to months, is in fact the continuation and dissipation, respectively, of the peak, only temporarily interrupted by the dip. As discussed in Sections 3 and 4, it seems that the higher the peak is, the brighter the dip minimum, the brighter the egress-maximum, and vice versa. If this picture of the egress-maxima is correct, the asymmetry of the dips can be explained. The observed slow egress phase results from two competing effects: the decline of the peak after maximum brightness and a steeper egress than observed. This does not rule out the possibility that the dip is also intrinsically asymmetric. The occasional absence of a clear dip in the optical (like after 1981.3, Fig. 1) is an indication that after the PP the duration of the optical peak was short, see Sect. 5.4.

We expect that for some photometric events the true maximum of the peak occurs after the PP, thus, much later than the observed one, but the dip prevents seeing its precise location. In this way the extremely high egress-maxima relative to the maxima of the peaks of the 2003.5 event, especially in H and J (see spline fits in Figs. 4–7) and in V (Fig. 1), can be explained. The assumption above offers also an explanation for the observed asymmetry of the peaks with respect to the PPs. After all, one may expect that after a period of brightening due to e.g. some kind of process by tidal forces, more or less the same time is required to normalise after having reached a climax. However, on a time scale longer than a few hundred days after the PPs, light and colour behaviour will inevitably be influenced by the long-term stellar brightness variations.

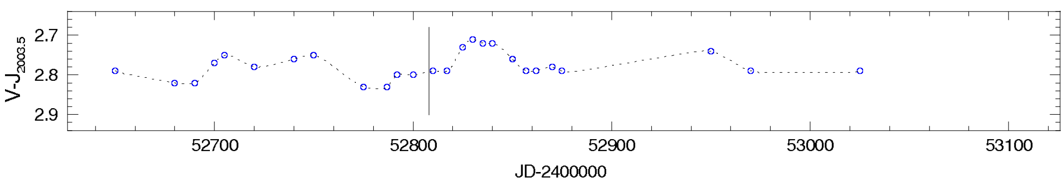

Figure 9: The $V-J$ colour curve of the 2003.5 event. The verical line represents the PP.

5.3 The long-term oscillations

Several attemps have been made to explain various features in the light and colour curves as due to S Dor-type oscillations with a time-scale of 1–3 yr, occasionally associated with shell ejections. With respect to the mass ejections, episodic excess-radiation in certain passbands was observed as the result of a collision of ejected material with a disk or with existing condensations a few hundred AU from the star (van Genderen et al. 1994). This picture fits into the HST-based studies on all kinds of physical and dynamical processes in and close to the core. The analysis of the new observations in the present paper does not alter much of these points of view, also with respect to the S Dor-type oscillations (which are very weak, not more than $0\overset{m}{.}1$–$0\overset{m}{.}3$). In Sect. 5.7.3 we shall demonstrate that the long-term brightness depression from 1994 to 1997 also bears the signature of an S Dor-type variation, and that it is quite different from the secular brightening and the post-egress brightenings.

The light curves in Sects. 3 and 4 show that at least a year prior to the periastron passages, a slow reddening is seen in $B-V$, $b-y$ and in $J-H$ until the PP ($0\overset{m}{.}05$–$0\overset{m}{.}1$). Subsequently, $J-H$ becomes bluer during several hundred days. A blueing episode in $B-V$, right after the PP is interrupted by a new reddening episode, until two to four months after the PP (Fig. 3). A shell ejection could cause such a temporarily reddening episode after the PP. Indeed, a spectral analysis of HST observations during the 2003.5 event strongly suggests some kind of mass ejection (Stahl et al. 2005).

A reddening trend accompanying a brightness rise is typical for an S Dor-type expansion phase of a star, also in the NIR. In the case of η Car, $U-B$ is not always a valid observable, because of the disturbing short-term UV oscillation (Sect. 5.8.2), and $H-K$ and $J-L$ are peculiar as well (Sect. 5.1). However, one should not forget that part of the observed reddening trends towards the PP may be due to the phase-locked fading of emission lines. After all, the blue band contains more emission lines than the visual (see the spectra at low and high resolution, i.e. near the periastron, and high states, i.e. outside periastron, Damineli et al. 1998). Phase-locked colour variations in the NIR, as described in Sect. 4.4, were already noted by Whitelock et al. (2004).

As a matter of interest we show in Fig. 9 the colour index $V-J$ for the 2003.5 event from the start of the peak until 200^{d} after the PP (V from Fig. 1, J from Whitelock et al. 2004, both light curves were read off at appropriate time intervals). The $V-J$ curve is bumpy like both light curves, but much more than the other colour curves. The bumps in V and J are apparently not concordant. The reddest colour occurs just before the PP, the bluest colour occurs roughly at the same time of the blue bump in $B-V$ (Fig. 3). We conclude that the $V-J$ curve agrees with the $B-V$, $b-y$ and $J-H$ curves in various respects.

As no conspicious spectral variations are found during the light oscillations, some authors doubt that η Car shows S Dor-type variations at all. Stable (i.e. 'ex-/dormant') S Dor-type stars do exist (van Genderen 2001), but η Car's very weak light oscillations are in no way comparable to those of e.g. S Dor, AG Car, HR Car, etc.: 1–2.5 mag, thus the absence of conspicious line variations during the long-term light oscillations is not alarming.

We conclude that S Dor-type variations, during which the star often reaches maximum expansion during a PP, are a likely explanation for a number of long-term light oscillations (see also Sect. 5.7.3).

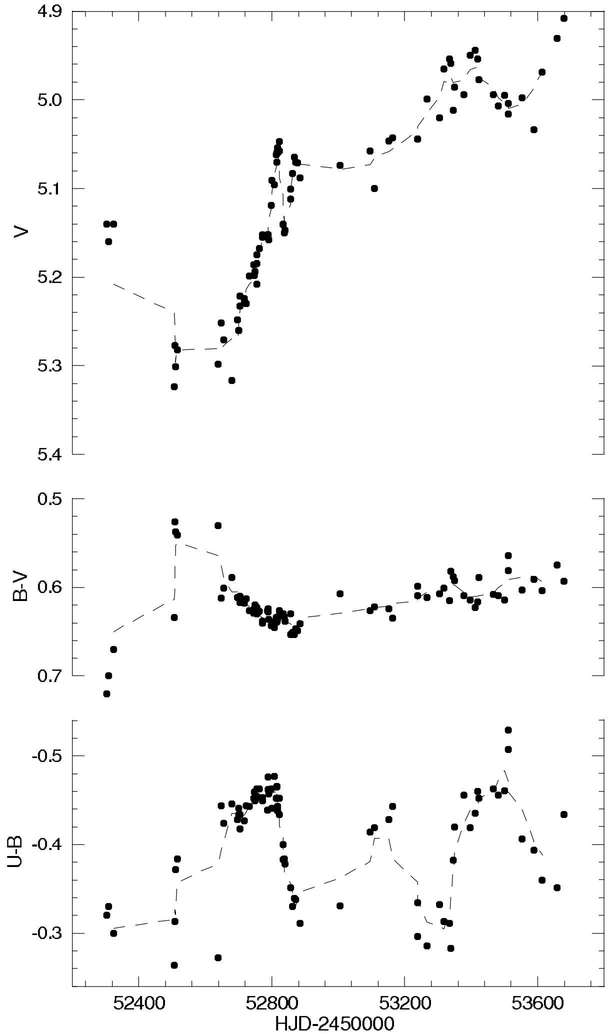

Figure 10: *UBV* light curves for the 2003.5 event until 2006 showing the post-egress brightening (based on Allen et al. 2005, but with slightly different V and $B-V$ scales, and a substantial improvement of the $U-B$ scale, see Sterken et al. 2006). The dashed line is a running average.

5.4 On the cause of peaks

If the interpretation of most long-term light oscillations as S Dor-type phases is correct, the absence of strong discontinuities in $B-V$, $b-y$, $V-J$ and $J-H$ during the photometric events suggests that the peaks can be considered as a continuation of the primary's expansion. Additional complicating effects on light and colour variations during the PP are, for example, tidal bulges, reflection effects on the primary by the hot companion, increasing asymmetry of the wind (e.g. Viotti et al. 1998), variable aspect angle by the binary revolution, increased mass loss rate, etc. With respect to the last item we refer to evidence supporting some kind of mass ejection during the 2003.5 event (Stahl et al. 2005). These authors also describe the fading of H, He, FeII emission lines during the decline to the dip as a rapid ingress and slower egress phase like the brightness in all photometric passbands. In the wind-wind collision model of Falceta-Gonçalves et al. (2005), the wind behind the shock mimics a shell ejection episode which can explain various features during the events. Suppose that the long-term light oscillations discussed in Sect. 5.3 are indeed due to a mix of an S Dor-phase and a shell ejection, one may wonder whether the light peaks represent the lift-off phase of the shell. Further, one should question whether the reddening episodes of $B-V$, $b-y$ and $J-H$ lasting up to 2–4 months after the PP, suggest cooler gas in front of the star. In the light of such a model, the occasional absence of an egress in the optical after the decline, is an indication that the peak has already disappeared. It is tempting to speculate that the optically radiating layers of the star contracted back to 'normal', thus, to its pre-peak position, contrary to the outer NIR radiating layers in an expansion phase. The latter also explains the more outspoken NIR egress-maxima and the strong discontinuities in $J-L$ and $H-K$ which suggest a temporarily strong fading of free-free emission (see next Section for an explanation).

5.5 On the cause of the dips

Martin & Koppelman (2004) noted that no dip appeared in the narrow-band 6770 Å and HRC/F550M photometry of the central star's continuum during the 2003.5 event, and they concluded that the dip is probably not caused by a weakening of the primary star. This agrees with our conclusion based on the normal depth of the dip in R (the obscured body is not a strong Hα radiator). On the other hand, the dip in the far-UV seems to be due to weakening of the FeII emission lines (Martin & Koppelman 2004), which very well could come from the atmosphere of the primary, if its temperature is not too high. We presume, also in view of the trend of the dip depths in Fig. 8, that two or more emitting regions are more or less simultaneously obscured/weakened, thus making a mixed impression: radiating in continuum light (e.g. by free-free radiation and warm dust), and also strongly in emission lines (e.g. FeII).

One can easily suspect that, somehow, an obscuration phenomenon or an eclipsing process of the secondary and its emitting circumstellar matter is responsible for the dip. This matter could consist of a wind envelope, shock fronts, a trailing wake behind the secondary, an equatorial disk, or other effects (see also Hillier & Allen 1992; Damineli et al. 1998; Steiner & Damineli 2004).

Based on photometric characteristics, the presence of a bright disk somewhere in the system was suspected[2] (van Genderen et al. 1994). Soker (2003, 2005) discussed the creation of an accretion disk in the binary.

With an inclination angle of 45°, a genuine eclipse of the secondary is perhaps not possible. However, if the primary's (polar) wind is dense enough, obscuration can be expected only if the secondary is in conjunction during the PP (this configuration is suggested by, e.g.

[2] Though, the tentative model with a short-period binary is abandoned, see Sect. 5.8.2.

Table 1: The magnitude differences between the obscured emission sources and the two stars (i.e. the relative energy distribution of these sources) for three PPs. It is assumed that the brightness of the two stars is represented by the dip minimum, and that the total brightness of the system is given by the peak maximum.

band	1981.3	2003.5	band	1997.9
U	2.15	1.93	*u*	1.86
			v	2.94
B	2.54	2.54	*b*	2.79
V	2.66	2.54	*y*	2.54
R		2.43		
I		2.33		
J		2.00	*J*	2.33
H		1.80	*H*	1.86
K		1.52	*K*	1.57
L		1.37	*L*	1.36

Ishibashi et al. 1999; Steiner & Damineli 2004; Akashi et al. 2006)[3]. After all, the far-UV emission spectrum of the secondary was also absent on July 27, 2003 (JD 2452818) and still a week later – thus, 2–3 weeks after the 2003.5 PP (Iping et al. 2005). Steiner & Damineli (2004) also suggested the possibility that the polar wind of the primary is responsible for the eclipse of the HeII emission, of the equatorial disk and of the X-ray emitting shock front.

However, it is not yet clear how such an obscuration process should be explained physically. The absence of a dip in the visual continuum (Martin & Koppelman 2004) implies that at least the secondary's visual continuum is hardly affected. However, if this obscuration works, it should happen close around the PP because of geometrical reasons and as long as the polar wind along the line of sight is dense enough.

That an enhanced polar wind in η Car most likely exists, follows from observations (Damineli et al. 1998; van Boekel et al. 2003; Smith et al. 2003b) and from a theoretical model (Dwarkadas & Owocki 2002).

The far-UV dip (Martin & Koppelman 2004) may be caused by recombination of FeII atoms in the atmosphere of the primary facing the earth, and/or in the nebular "Weigelt blobs" BCD as soon as the hot secondary is shielded by the primary's wind (see also Davidson et al. 1995, 2005; Hartman et al. 2005).

If we assume that the dips are mainly due to a total obscuration of the secondary's emission features (line and free-free), then one can infer their wavelength-dependent magnitude differences relative to the two stars. This result will be independent of the foreground reddening and the secular brightening. Like the wavelength-dependent dip depths, such an attempt gives us some information on their relative energy distribution. The maximum of the peak represents the total brightness of the system, the minimum of the dip represents

[3]Note that also models exist with the secondary in front during the PPs (e.g. Davidson et al. 2000; Falceta-Gonçalves et al. 2005).

the two stars only. Transforming the magnitudes to absolute fluxes and subtraction of both fluxes yields the required magnitude differences (though slightly affected by the presence of the peak). This could only be done for the well-sampled events of 1981.3 (in the optical), 1997.9 and 2003.5 (both in the optical and NIR). These differences are listed in Table 1. They closely follow the opposite trends of the dip depths in Fig. 8, with largest difference in the blue ($2\overset{m}{.}8$), a decreasing magnitude difference to the UV ($1\overset{m}{.}9$), and the NIR ($1\overset{m}{.}4$). Even if the obscuration is only partial, this relative energy distribution indicates that we are dealing with various types of obscured radiation sources, thus with much UV radiation (FeII emission) and even with more NIR radiation. It is unlikely that the dip is caused by dust extinction alone, as suggested by Falceta-Gonçalves et al. (2005), considering the trend of the dip depths in Fig. 8. The stability of these magnitude differences at the three events is remarkable, and indicates that the luminosity of the primary is not noticeably variable.

A successful model for the X-ray emission cycle is presented by Soker (2005b) and Akashi et al. (2006), in which the secondary wind, hence the X-ray source, is shut down shortly after the PP. This model offers two possibilities for the orientation of the system. If the cause of the dip is as proposed above, orientation B is applicable (see Fig. 5 of Akashi et al. 2006). This orientation is also preferred by Steiner & Damineli (2004). Figure 11 represents a schematic drawing of such a configuration with a number of important features marked with the Julian Date. As can be seen, the dip occurs after the PP in the first half of the X-ray minimum.

As noted above, the far-UV emission spectrum of the secondary was absent on July 27, 2003 (JD 2452818). At the same time the NIR declines started (JD 2452810–2820), suggesting a causal connection: the secondary, obviously, had entered the primary's wind. While it moved away to the back side, the optical decline started (JD 2452823), but it shared the same time for the minimum brightness with NIR (JD 2452840) indicating that most of the radiation in this spectral range came from one single system. This climax was reached when the system of the secondary was supposed to be blocked by the polar wind of the primary. If it was a total "atmospheric eclipse", the upper limit for the visual brightness difference between the two stars and the circumstellar structure was about $2\overset{m}{.}5$ (Table 1). According to Verner et al. (2002), the secondary has $M_{\rm bol} = -10.2, T_{\rm eff} = 37200$K, thus $M_V \sim -7$. As $M_{\rm v}$ of the primary is -9 to -10, $M_{\rm v}$ of the emitting circumstellar structure lies between -6.7 and -7.6, thus of the same order as the secondary itself.

We presume that the radiation deficit in K and L starting a few months before the PP is caused by the partial annihilation of the source by the outer envelope and wind of the secondary during the close encounter. This scenario is in agreement with Soker's (2005b) flow model of the accretion process by the secondary with the result that its wind practically ceases to exist for a short time. Soker (2005b) and Akashi et al. (2006) conclude that "the previously colliding wind region collapses onto the secondary".

From the $H-K$ and $J-L$ color curves (Figs. 4, 6, and Fig. 3 in Whitelock et al. 2004), we deduce that somehow the K and L radiating matter around the secondary needs a year or more after each PP to build up again. In Sect. 5.2 we noted that if the obscured body would be the main contributor to the Hα radiation, the dip depth in R would have been larger than in the adjacent bands, and this was not the case (Fig. 8). However, in the above scenario possible H-emission by the secondary should also cease during the PP, then contributing partly to the observed emission decrease of H-lines and their slow recovery after 2003.5.

This Section illustrates once more, how important future ground-based photometry – in combination with other observing techniques – will be for the study of what actually happens in the core during the PPs.

5.6 The amplitudes of peaks and dips are independent of the Humunculus brightness

The size of the peaks in magnitudes seems to be independent of η Car's steadily growing apparent brightness. The amplitudes of the 1981.3 and 2003.5 peaks are almost equal, while the brightness prior to the 2003.5 peak was $0\overset{m}{.}7$ in V and $0\overset{m}{.}8$ in J higher than prior to the 1981.3 peak. On the contrary, the 1981.3 peak was almost twice as large as the one of 1997.9 peak ($0\overset{m}{.}19$ versus $0\overset{m}{.}11$ in V, $0\overset{m}{.}20$ versus $0\overset{m}{.}13$ in J), while its pre-peak brightness was fainter by $0\overset{m}{.}4$ in V and $0\overset{m}{.}6$ in J.

The sequence 1992.4, 1997.9 and 2003.5 would suggest a dependency of the peak amplitude (e.g. $J = 0.06, 0.13$ and 0.21, respectively) and brightness ($J = 2.93, 2.83$ and 2.49, respectively). This can very well be accidental. Supposing that the primary is indeed subject to (very weak) S Dor phases, the peak size could depend on the geometrical state of the primary, i.e. its radius. A larger radius and, consequently, a lower surface gravity would make the star more sensitive to tidal forces. The 1981.3 event is indeed located on top of a high local maximum, contrary to the events of 1992.4 and 1997.9 (van Genderen et al. 1994; Sterken et al. 2001a,b). The situation during the 2003.5 event is difficult to estimate.

Thus, the peak heights fluctuate around an average $\sim 0\overset{m}{.}15 \pm 0\overset{m}{.}05$ in V, and $\sim 0\overset{m}{.}15 \pm 0\overset{m}{.}07$ in J which seems to be independent of the steadily-growing apparent brightness ($0\overset{m}{.}7$ in V between 1981.3 and 2003.5, thus by a factor of two in flux). If this would be due to an intrinsic brightening of the primary, the average flux of the peaks should have grown by a factor of two as well. Furthermore, the dip depths should have been shallower by a factor of two (assuming that the dip is not due to an eclipse of the primary, see Sect. 5.5), which is clearly not the case. On the contrary, the dip depths ($\sim 0\overset{m}{.}1$ in V) appear to be more stable than the peak heights (Fig. 8).

We conclude that, so far, peak heights and dip depths are independent of the increasing apparent brightness of η Car. More confirmation is needed by analysing future peaks and dips. In short, we conclude that the luminosity of the primary has not noticeably changed over the last 35 years.

5.7 The secular and post-egress brightenings after 1997.9 and 2003.5

5.7.1 The brightening rates

The secular brightening appears to be almost linear for the interval 1952–1992, its rate in V is $0\overset{m}{.}025\,\mathrm{yr}^{-1}$ (van Genderen et al. 1994). From 1992 to 1997.9 the rate is linear as well (see further), but the linearity is interrupted by the two post-egress brightenings after the event of 1997.9 (Figs. 5, 7), and the one after the 2003.5 event (Fig. 10). The rates for the secular brightening given by Whitelock et al. (2004) cannot be used as they are too high because these rates include the two post-egress brightenings.

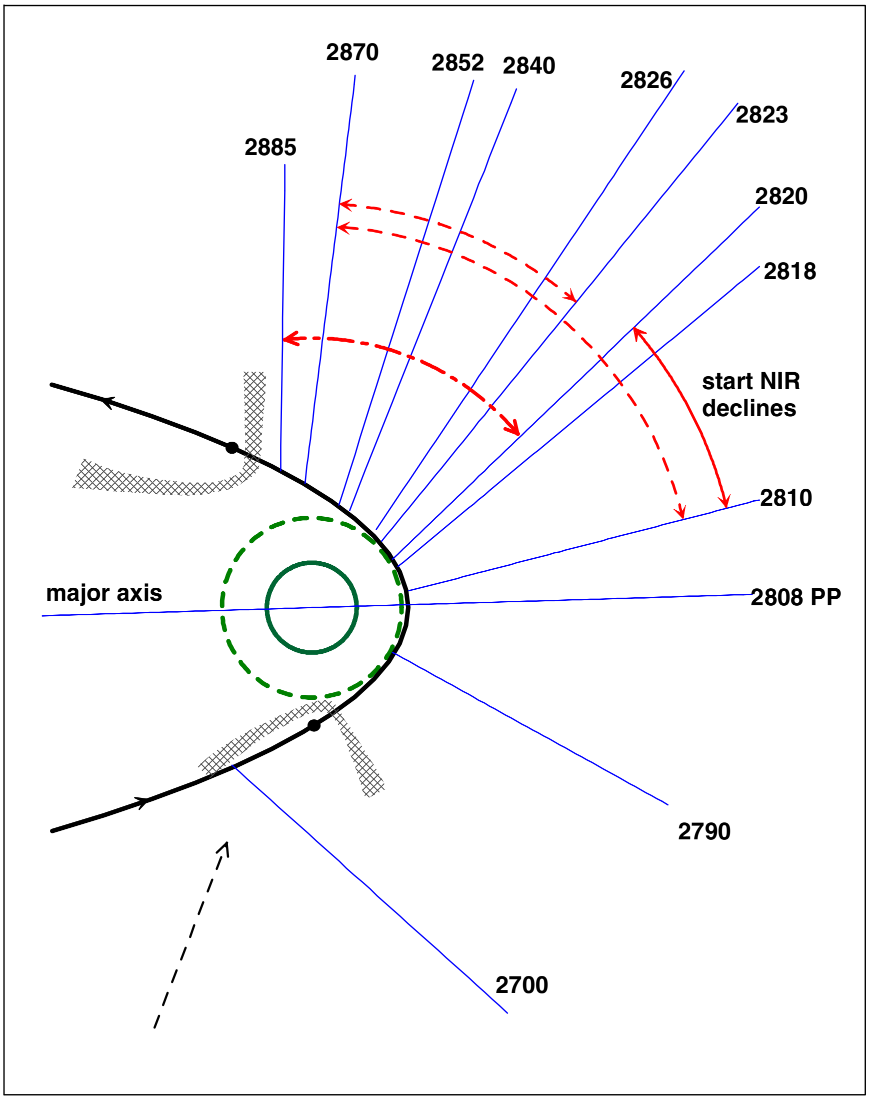

Figure 11: A schematic drawing of the binary system (seen pole-on, with a viewing angle of 45° and not to scale) based on (the also schematic) orientation B by Akashi et al. (2006). Circle and small dot: the primary and secondary, respectively. Large circle (dashed): the wind envelope of the primary. Hatched area: the shocked secondary wind. A number of features are indicated by time marks (JD-2450000): 2700 (start peak in optical and NIR); 2790: start X-ray decline; 2808: PP; 2818: far-UV secondary absent; 2823: start optical decline; 2826: far-UV secondary absent; 2840: minimum dip optical and NIR; 2870: post-egress maximum. Short and long dashed arrow arcs: duration of dip in the optical and NIR, respectively. The dashed-dotted arc represents the X-ray minimum.

Table 2: The rate of the secular brightening in m yr^{-1}, in UBV, $JHKL$ and $VBLUW$.

Band	1952–1992	1972.09–1997.78	Band	1974.24–1991.16
U		0.021	*W*	0.032
B		0.018	*U*	0.034
V	0.025	0.021	*L*	0.034
J		0.025	*B*	0.028
H		0.033	*V*	0.027
K		0.025	*J*	0.025
L		0.004	*H*	0.035
			K	0.027
			L	0.006

Table 2 lists the rates of the secular brightenings for two largely overlapping time intervals, viz. 1972.09–1997.78, and 1974.24–1991.16. These portions were selected in such a way that two types of optical photometry (UBV and $VBLUW$) and the simultaneously obtained $JHKL$ photometry are complete. The first time interval ends just before the start of the light peak belonging to the 1997.9 event. Of course, small inconsistencies can be introduced by the stellar variability, affecting the first and last observations, especially in the UV, unless the oscillations are well sampled and a reliable average trend can be determined like after the 2003.5 event (Fig. 14).

Fig. 12, left panel, shows the wavelength dependency of the brightening rates for the secular brightening for the two time intervals above. Different start and end points do not alter the trends in the NIR, but somewhat affect the trends in the optical. The optical rates for 1972.09–1997.78 are lower than for 1974.24–1991.16, and the last interval shows an additional UV bump. The reason for the low optical rates in the first interval is that the long-lasting brightness depression 1994–1997 is included (van Genderen et al. 1999; Sterken et al. 2001a,b).

The UV bump mentioned above is caused by the pronounced activities in the near-UV (in excess of $0\overset{m}{.}1$ on top of the normal light variations) measured in the medium-broadbands of the $VBLUW$ system: L (higher Balmer lines and Balmer limit), U (Balmer jump) and W (Balmer continuum), in particular between 1978 and 1980 (in W) and in 1987 (in L and U, Figs. 4a,b in van Genderen et al. 1994).[4]

It is reasonable to assume that for the total time interval of 45 yr, 1952–1997.78, the average of the trend from J to the UV runs somewhere in the middle of the two relations in Fig. 12, left panel. The 1952–1992 rate in V ($0\overset{m}{.}025\,yr^{-1}$) supports this assumption. Therefore, we assume for the interval 1952–1997.78 the same visual brightening rate.

Table 3 also lists the post-egress brightening rates after the 1997.9 and 2003.5 events. There is a fast part: 1998.24–1999.06 (JD 245 0900–JD 245 1200) in *uvby* and $JHKL$ (we

[4]In the first interval these near-UV activities are leveled out by the inclusion of the brightness depression 1994–1997. These strong emission episodes, particularly in the H-lines and Balmer continuum, point to strong, but temporary changes in the gaseous surrounding of the primary.

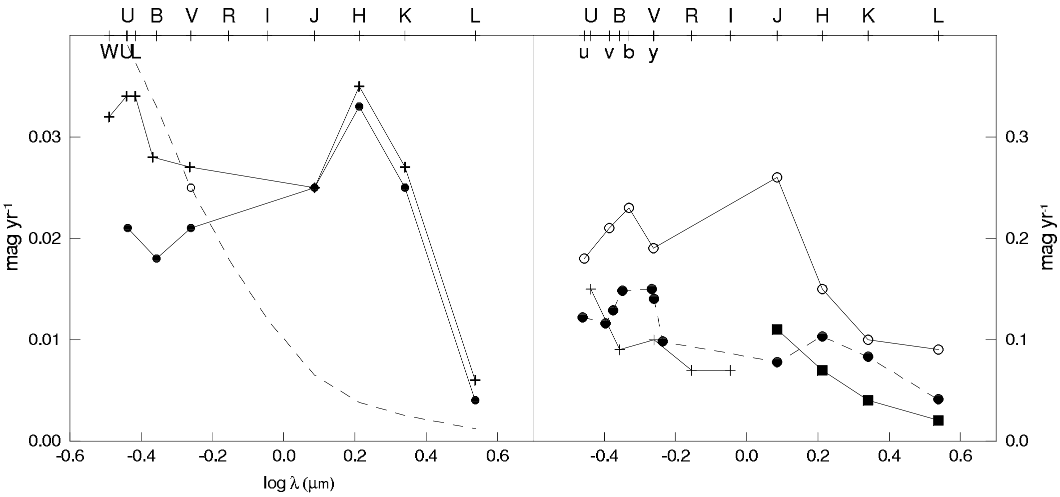

Figure 12: *Left:* the rates of the secular brightening in $\mathrm{m\,yr^{-1}}$, of the Homunculus as a funtion of the wavelength ($\log\lambda$ in μm). ○: 1952–1992 (V); •: 1972.09–1997.78 (UBV, $JHKL$); $+$: 1974.24–1991.16 ($VBLUW$, $JHKL$); curve: normal extinction law for a brightening rate in $V = 0^{\mathrm{m}}\!.025\,\mathrm{yr^{-1}}$ (○). *Right:* rates of the post-egress brightenings after the 1997.9 event, ○: the fast brightening 1998.24–1999.06 (*uvby*, $JHKL$); ■: the slow brightening 1999.06–2000.19 ($JHKL$), $+$: the brightening 2003.99–2005.35 (UBV, $BVRI$). The long-term oscillation prior to the 1997.9 event: 1996.26–1997.22 (Geneva bands and $JHKL$) represented by • and connected by a dashed line.

estimate that it started about 3 months after the PP) and a slow part: 1999.06–2000.19 (JD 245 1200–JD 245 1615), in $JHKL$ only. After 2000.19 no significant brightening was observed. The rates for the 2003.5 post-egress brightenings (started also about 3 months after the PP) for the interval 2003.99–2005.35 (JD 245 3000–JD 245 3500, short-term light oscillations averaged out by a straight line, instead of a running average as in Fig. 10). Note that the B and V rates are averages of the rates derived from the light curves from this paper (data from the Appendix), Lajús et al. (2003) and Niemela et al. (2005).

These rates are plotted as a function of wavelength in the right panel of Fig. 12 (note that the optical rates mainly represent the brightening of the Homunculus, and those for the NIR mainly that of the core, Sect. 4.4, see also further). These post-egress brightenings (optical to the NIR) are an order of magnitude faster than the secular brightening and also of a quite different character, at least in $JHKL$. On the contrary, the fast and the slow parts of the 1997.9 post-egress brightening show the same trend in $JHKL$, the first faster than the second by a factor 2–3. As optical rates (in $UBVRI$) are lacking for the slow 1997.9 trend, and $JHKL$ rates are lacking for the 2003.5 post-egress brightening, no comparison is possible.

Table 3: Rates of the post-egress brightenings (m yr^{-1}) after the 1997.9 and 2003.5 events.

filter	1998.24–1999.06	1999.06–2000.19	2003.99–2005.35
U			0.15
B			0.09
V			0.10
u	0.18		
v	0.21		
b	0.23		
y	0.21		
R			0.070
I			0.070
J	0.26	0.11	
H	0.15	0.07	
K	0.10	0.04	
L	0.09	0.02	

5.7.2 On the cause of the secular brightening

Interpreting the differences between both panels in Fig. 12, one has to account for two things. First: for the dichotomy that most of the NIR radiation comes from the core (Sect. 4.4; Allen 1989; Whitelock et al. 2004; Smith & Gehrz 2000), and most of the optical radiation from the Homunculus. Second: the secular brightening is such a slow process, that the logic consequence of the expansion of the Homunculus, viz. the thinning of dust, has to compete with other long-time scale processes caused by the same expansion.

The dashed curve in the left panel of Fig. 12 represents a normal extinction law (Savage & Mathis 1979) through the rate for *V* (1952–1997.78). Evidently, the secular brightening in the optical as well as in the NIR is far from being caused by an extinction decrease alone. It is even questionable whether the bulk of the NIR brightening (in the core) has been influenced at all by the expansion of the Homunculus.

The progressively lower brightening rate to the long wavelengths (*L* band) supports the fact that in *M* the brightness of the Homunculus is decreasing (van Genderen et al. 1994) as well as at 10 μm (Gehrz & Smith 1999).

A first attempt to explain the observed wavelength dependency of the secular brightening was made more than a decade ago (van Genderen et al. 1994). Apart from the thinning of dust (decrease of 'self-extinction'), the analysis included a decrease of reflected light and a decrease of the temperature of the dust by the expansion of the Homunculus. The dichotomy in the measured ground-based flux was still unknown. By the expansion all parts will gradually be illuminated more directly, giving rise to brightening and warming up of gas and dust up to the borders. This is a realistic assumption as Smith et al. (2003a) found that the lobes are optically thick, even to direct UV and optical radiation. Note that changes in the scattering and absorption characteristics of the dust depend on e.g. the mass and size spectrum of the dust particles, ruled by the irradiation and density changes. That this is a very complicated matter, follows from the study of Walsh & Ageorges (2000), who found strong discrepancies between the predictions of the extinction and the emission of grains and their polarization properties.

The peak in the *JHK* rates (left panel of Fig. 12) points to a faster change in the core than in the other channels, and we concur with Whitelock et al. (2004) that this is likely due to increasing free-free emission. Groh & Damineli (2004) noted a secular change in emission lines during the last two orbital cycles suggesting that the optical depth of the emitting region is indeed increasing. The most obvious conclusion is that the mass and size of the primary's wind envelope is steadily growing. Most of the measured NIR radiation comes from a small volume (see the beginning of this Section), but the gas will gradually expand further into the Homunculus. As the observed secular brightening in the NIR is linear, the mass loss of the primary per orbital cycle has been constant over at least the last 35 years.

5.7.3 On the cause of the post-egress brightenings of the central star and the Homunculus. The extinction law

Before exploring the post-egress-brightenings, it is of importance to underline that the long-term light oscillation of η Car prior to the 1997.9 PP is of a different character.

The cause of the pronounced post-egress brightening of the Homunculus after the 1997.9 PP was certainly not due to S Dor-type variations of the star. However, the *initial* (pre-periastron) rise from early 1996 to 1997.9 and sometime thereafter, probably was (Sterken et al. 1999a,b). It clearly bears the signature of such a type of variation: the colour indices reddened during the brightening. In the course of 1998 the $b-y$ index was clearly blueing, obviously a stronger process was overruling the S Dor-phase, or the latter stopped and reversed its cycle (van Genderen & Sterken 2004). To illustrate the reddening trend in the optical, we show in the right panel of Fig. 12 the brightening rates for the initial rise (1996.26–1997.22) in seven Geneva passbands as dots connected by a dashed line. The reddening trend from the UV to the visual is evident, but the jump down to the *G*-band ($\lambda = .581\mu$m, $\log\lambda = -0.236$) and the trend to *JHKL* is odd, indicating relatively low rates, thus implying low amplitudes. According to an analysis of two other long-term brightness waves of η Car (1981–1986) and of one brightness wave of AG Car, the amplitudes can also be larger at longer wavelengths (Fig. 8 in van Genderen et al. 1994). It is important to mention that the same trend, thus, similar to the dashed line in in Fig. 12 right panel, is found for the entire brightness depression divided in two other parts, viz. for the intervals 1994.39–1995.37 and 1995.37–1997.22 (thus, from the Geneva *U* band to the NIR *L* band).

Whatever the cause for the observed trend of the entire brighness wave 1994–1997 and other ones investigated by van Genderen et al. (1994), they are quite different from the post-egress and secular brightenings. It is not realistic to suggest that the gradual brightening which happened before 1997.9 was possibly due to dust clearing as the Homunculus expands (Smith et al. 2000). Not only because of the analysis above, but also because of the small effect of the expansion in such a relatively small time interval.

In order to explore the post-egress brightenings, the two brightening parts after the 1997.9 event in *JHKL* from the right panel in Fig. 12 are reproduced in Fig. 13 left panel,

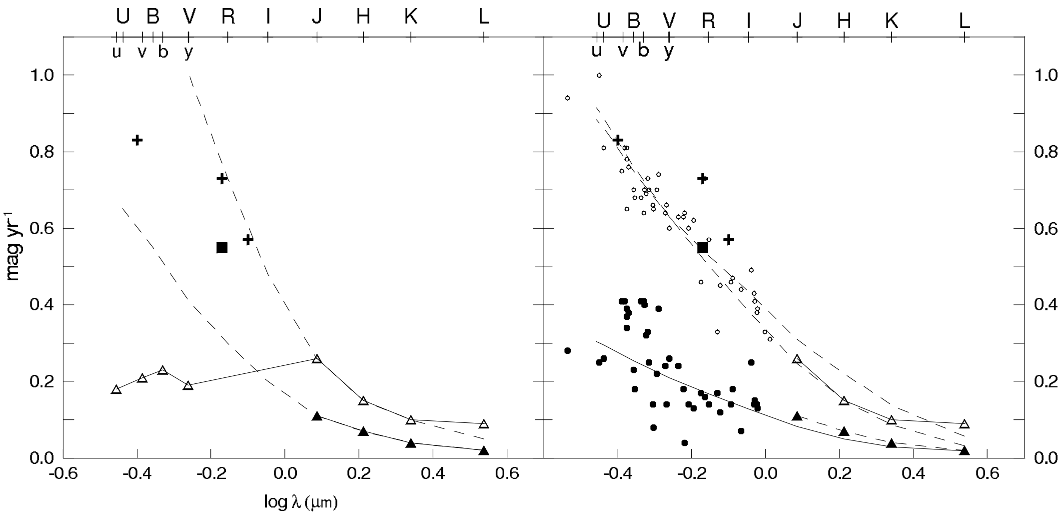

Figure 13: *Left*: the rates of the post-egress brightenings of the Homunculus after the 1997.9 event partly taken from Fig. 12 right panel. $+$ and ■: the brightening rates of the continuum fluxes of the isolated central star (HST/STIS) 1998.00–1999.14. Dashed curves are for a normal extinction law for $V = 1\overset{m}{.}0\,\mathrm{yr}^{-1}$ (upper curve), and $V = 0\overset{m}{.}41\,\mathrm{yr}^{-1}$ (lower curve). *Right*: $+$, ■, △, ▲: same as in the left panel (optical data are omitted). ○: the fast brightening rates of the stellar continuum 1998.21–1999.14; • : the slow brightening rates of the stellar continuum 1999.14–2000.22. Dashed curves: brightening rates for $R = 4.9$ and 5.3 (lower and upper curve, respectively) for the fast rates, and for $R = 4.9$ for the slow rates.

with a magnitude scale reduced by a factor two. The dashed curves – representing the expected trends if a normal extinction law is applicable (Savage & Mathis 1979) – fit the $JHKL$ data points surprisingly well (L in the upper curve slightly deviating). The corresponding rates in V are $1\overset{m}{.}0\,\mathrm{yr}^{-1}$ and $0\overset{m}{.}41\,\mathrm{yr}^{-1}$ for upper (fast) and lower (slow) curve, respectively. The post-egress brightening rates in the three HST/STIS narrow bands (4000, 6800 and 8000 Å) of the isolated stellar continuum are also plotted, as well as the HST/STIS narrow band 6770 Å rate. These HST observations of the central star were made in almost the same time interval as the optical and NIR data points for the fast part (upper curve) obtained from the ground. The good fit of the NIR and the 6800 Å and 8000 Å rates on the same (upper) curve is quite unexpected. The deviation of the 6770 Å rate with the 6800 Å rate on the curve is perhaps not alarming. However, the very large deviation of the 4000 Å rate with respect to the upper curve creates a problem. Apart from this, the good fit is quite confusing as most workers believe that no normal dust particles exist near the core (e.g. Robinson et al. 1987; Davidson et al. 1995; Hillier et al. 2001). Therefore, we wondered whether the good fit is accidental.

We investigated this problem further by consulting the spectrograms of the central star made at the three dates 1998.21, 1999.14 and 2000.22 (HST, Gull et al. 2001), thus, almost at the same dates as for the photometric observations discussed in Sect. 5.7. Stellar-continuum fluxes at 44 selected wavelengths from log $\lambda = -0.450$ to 0.012μm were transformed to magnitudes. The brightening rates (in m yr^{-1}) in the two intervals were derived and plotted in Fig. 13 (right panel) for the fast (the first interval) and for the slow (the second interval) part of the brightening (ground-based optical rates as well as the relation for a normal extinction law are not plotted in this panel).

Although Gull et al. (2001) attempted first-order correction for zero point drifts, there still are spectral overlaps showing small changes. Therefore, among the 44 fluxes we also have included fluxes at 11 overlapping wavelenghts resulting in two slightly different rates which were averaged. The majority of the mean standard errors (σ) for the fast rates turned out to be $\pm$ 0.^{m}04 yr^{-1}, only a few are more than 0.^{m}1 yr^{-1}. For half of the slow rates, the standard deviations are larger than 0.^{m}1 yr^{-1}. The plusses and the square mentioned above fall within the range of the scatter of the new data points of the fast part of the brightening of the central star *and* the Homunculus. After all, the global thinning of dust around the core responsible for the simultaneous 0.^{m}3 brightening of the Homunculus (after 1997.9) likely takes part in the NIR brightening rates in Fig. 13 right panel.

An anomalous extinction law fits the entire sample best. The two dashed curves for the fast rates are for $R = 4.9$ and 5.3 (V rate is 0.^{m}63 yr^{-1}) and are based on the calculations of anomalous extinction laws by Steenman & Thé (1989), assuming $E_{B-V} = 1$. The 4.9 curve fits best. For the slow rates only the $R = 4.9$ curve is shown (V rate is 0.^{m}21 yr^{1}). Thus, it seems that a decrease of large particles is responsible for the post-egress brightening of the central star and the Homunculus. It is well-known that anomalous extinction laws with high R values do occur around hot stars. Large particles near the core of η Car were suspected before (e.g. Davidson et al. 1995; Walsh & Ageorges 2000) and are supposed to be easily formed in a slow and dense outflow (Soker 2000, 2005a). Small particles seem to be predominantly present elsewhere in the Homunculus (e.g. Robinson et al. 1987; King et al. 2002).

The result above also demonstrates that the bulk of the NIR radiation is concentrated to the core, thus, ground-based observations in the NIR imitate to a certain extent small-aperture photometry. It is a fact that the NIR morphology of the core was more point-like around 1998 than some years earlier (Smith & Gehrz 2000). The minimum brightness of the dips in L and K also suggest a strong concentration to the core (Sect. 4.4), as well as the 2.39 μm observations by van Boekel et al. (2003). As the degree of concentration will not be 100%, we believe that if the NIR fluxes would have been measured with a small aperture, the $JHKL$ rates would have been higher. The reason is that these NIR fluxes would have been affected by the decreasing excess-extinction in the line of sight as well. Therefore, it is possible that the extintion law is higher than 4.9, closer to 5.3. Thus, one would conclude that the total foreground extinction to the core is $A_V = 5$. As in early 1998 $A_V = 7$ (Hillier et al. 2001), we must adopt an extra component having two magnitudes of grey extinction at that time.

We find more support for ‘excess-foreground extinction decrease’ (van Genderen & Sterken 2005) by space-based photometric evidence which also happens to support the mimicry of the Homunculus. Smith et al. (2000) list in their Tables 2 and 3 HST photometry made with 0.″14 (isolated central star) and 20″ (Homunculus) data at three dates in the red F631N band (JD 244 9982, 245 0608 and 245 1342).

The first interval runs from the minimum of the 1994–1997 brightness depression to

178 d prior to the PP of 1997.9. The brighness increase in red light of the central star is equal for both apertures, viz. $0\overset{m}{.}16$, roughly equal to the $0\overset{m}{.}15$ visual rise from ground-based photometry (e.g. Sterken et al. 2001a, b). Consequently, this example also shows that the Homunculus imitates the variations of the star very well, leaving no other option than to assume that a temporarily high excess-extinction episode in front of the star existed likely already for many years, which gradually disappeared in the course of 1998 to 2000. The Weigelt blobs BD lying closer to us than the star, suffering from much less extinction than the star (Hillier & Allen 1992), have maintained nearly constant fluxes in the WFPC2 images around 1998, while the star brightened by a factor of two (Gull et al. 2001). This inconsistency can easily be explained if the excess-extinction in the sight line to the star decreased, for example if an isolated dust knot moved out of the sight line between 1998 and 2000, hardly affecting our view to these blobs. *The decreasing brightening rates of the central region by increasing apertures as found and discussed by Smith et al. (2000), are now also understandable.*

However, we have no idea where such a hypothetical dust knot should have come from and why it happened simultaneously with the permanent brightening of the Homunculus by $0\overset{m}{.}3$. Further, it should have moved radially outwards as transverse movements seem to be impossible (Davidson et al. 1999). One should also expect more of them on statistical grounds, all moving outwards as if they were ejected from the core. We also believe that this dust knot theory is only realistic if it subtended an angle at least as big as the NIR core.

This excess-extinction in the line of sight to the star should have been there at least for years, since it was also present during the brightening phase of the Homunculus a couple of months before the 1997.9 event (see above) when also HST photometry of the isolated star was made, considering the magnitudes at the three dates listed above. Perhaps it simply was part of the dust shell encompassing the core.

The second interval (1997 June 8 – 1999 June 12, time interval 734 d) covers part of the pre-PP interval (178^{d} prior to the PP, still with no decrease of excess-foreground extinction, see below) and overlapping the entire fast and partly the slow brightening episodes. Consequently, its brightening rate is not comparable to the ones plotted in Fig. 13 right panel, and therefore not shown. The fact that the brightening of the star by the excess-extinction occurred more or less simultaneously with the brightening of the Homunculus (the latter happened 3 months after the PP), one may wonder whether a causal connection existed between the PP on the one hand, and with the brightenings of the central star and the Homunculus on the other hand.

The total visual extinction of the material responsible for the excess-extinction decrease in the line-of-sight of the central star, taking a time scale of 2.3 yr, by a brightening rate $0\overset{m}{.}63\,\mathrm{yr}^{-1}$ (for 1997.9–1999.14) and $0\overset{m}{.}21\,\mathrm{yr}^{-1}$ (for 1999.14–2000.22) should have been $\sim 0\overset{m}{.}7$, after subtraction of $0\overset{m}{.}3$ visual extinction decrease close around the core (see below).

It still leaves us to explain the ground-based optical brightening rates of the Homunculus. They represent the brightening of the Homunculus after the alleged dust clearance around the core by $0\overset{m}{.}3$ (early 2000) and an additional $0\overset{m}{.}25$ (end of 2005), respectively. These values are lower than those of the central star, because the brightness of the Homunculus was not affected by the decrease of the excess-extinction in the line of sight to the star.

But do these values truly represent the visual extinction decreases around the core? In other words, is the mimicry of the Homunculus in the optical also valid for this type of process and for all optical wavelenghts? The reason to pose these questions is the following: there is no consistent trend in the optical brightening rates (a zig-zag pattern from the visual to the UV for the 1997.9 event, and from the red to the UV for the 2003.5 event). These trends are hardly suitable for finding a reliable extinction law. Moreover, it is not known which rate in what filter is reliable and which one is not. Nevertheless, if we derive the extinction law from a mean curve sketched through the red up to the UV rates of the brightening after the 2003.5 event, we find $R \sim 5$. Although crude, this value for the dust clearance around the core does not contradict the result from Fig. 13 right panel. The extinction decreases imply that if an extinction to the core of 7 magnitudes in early 1998 is correct, A_V should have been 6 in early 2000, and 5.7 early 2006.

The possible causes of the problematic optical brightening rates (Homunculus) due to a global dust clearance close around the core are:

1. All kind of spectral variations from the core which are wavelength dependent, detoriating the optical rates of the Homunculus.

2. Heating and illumination of the dust and gas complexes will become more intense, inevitably influencing the scattering and the emission properties of the dust and gas, up to the borders of the Homunculus. This might result in a varied and not consistent effect on the wavelength-dependent behaviour of the optical brightening rates. This is contrary to the weak light oscillations of the primary, or of other features in the core ($< 0\overset{m}{.}3$) as they show a weak wavelength dependency (small colour variations).

In this way the zig-zag pattern in the optical secular, and post-egress brightenings, might be explained. With respect to the secular brightening rates in the optical: one of the effects of the expansion of the Homunculus, including the inner parts, is also the more direct heating and illumination by the two central stars (partly cancelling, or even overruling the cooling by the increasing distance from both stars). They will suffer from the same repercussions as outlined in point 2. with that difference, that all the processes happen on top of a very slow density decrease of the material in the Homunculus. We do not claim that the above offers the right explanations, but at the moment we cannot find other ones.

5.8 The UV continuum oscillations

Like in other spectral regions, the binary period left its footmarks in the ground-based observations during a few binary cycles in the eighties and nineties of the previous century. At the same time a second much shorter oscillation, apparently only in the Balmer continuum is superimposed (van Genderen et al. 1999, 2001). As smearing-out of radiation from the core of η Car by the Homunculus appeared to be negligible (Sect. 1 and 5.7), these UV oscillations need to be taken seriously.

The analysis of a couple of decades of multi-colour photometry suggested the presence of luminous circumstellar matter close to the binary, or as a disk around one of the components, likely in the equatorial plane (van Genderen et al. 1994). This is supported by observational evidence and models by e.g. Damineli et al. 1998; Gull & Ishibashi (2001), Balick & Matt (2001), Soker (2005a,b), Abraham et al. (2005) and Akashi et al. (2006).

5.8.1 The binary-related oscillation

With respect to the binary-related oscillation, we presume that it is due to modulated H-emission, alternately radiating in excess of the stellar radiation, in lines (outside periastron) and in the Balmer continuum (during periastron). The $J-L$ and $H-K$ discontinuities, suggesting a probable temporarily decrease of free-free emission, are likely related with this phase-locked orbital variation (Sect. 5.1). In Figs. 7 and 8 of van Genderen et al. (1994), the Walraven colour indices $W-B$ and $U-B$ are used. The W band is very suitable to measure fluctuations in the Balmer continuum area like the Strömgren u and the Geneva U bands, provided that other light variations are largely eliminated by taking the colour indices $W-B$, $u-v$, etc. η Carinae's colour variations of most light oscillations turned out to be indeed small.

Peaks in $W-B$, as high as $0.^{m}15$, were noticed during the 1981.3, 1986.8 and 1992.4 PPs. Midway the next PP, when the $W-B$ peak faded away, a peak arose in the Walraven $U-B$. This was explained by a physical change of a luminous disk being optically thick at periastron and optically thin outside of it. The 1997.9 PP showed a problematic result: only the light peak is present, but not the 'excess-Balmer continuum radiation' peak (Fig. 8 in van Genderen et al. 1999). This happened again during the 2003.5 PP (van Genderen et al. 2003b; Allen et al. 2005), and has happened during the 1975.8 PP (Fig. 7 in van Genderen et al. 1999).

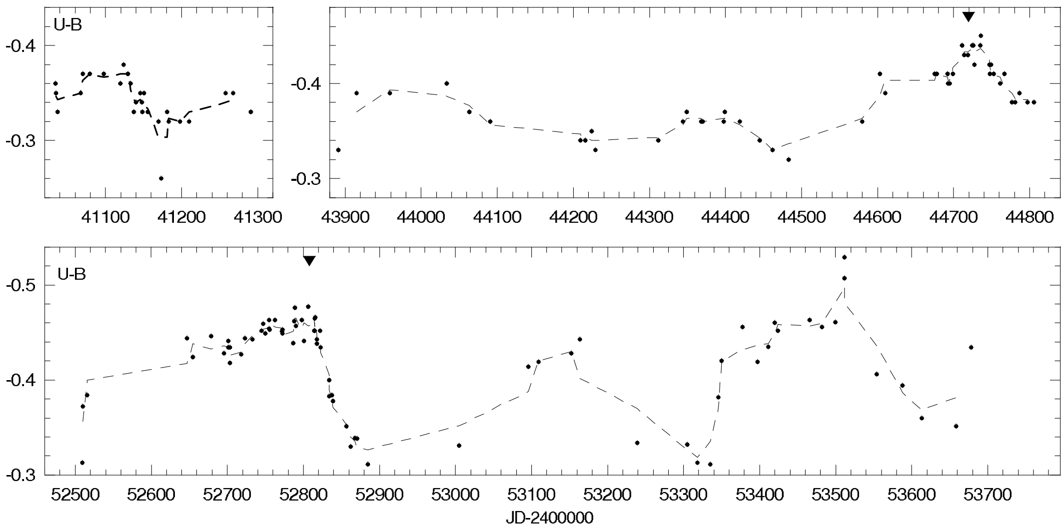

Figure 14: Sample $U-B$ curves showing the 'few-100^{d}' oscillation. 1981.3 and 2003.5 PPs are indicated with ▼ (data from Walker and Allen, see Appendix). Upper panels: 1972 and 1979–1981. Lower panel: 2003–2006.

Note that the Johnson $U-B$, due to its large width, is not suitable to bring this oscillation to light. As Johnson U includes the much narrower Walraven passbands W, U and L, the alternating flux variation from W to UL, results in an almost cancellation of these flux variations in the broad band. This is very well illustrated in Fig. 14, showing the Johnson

$U-B$ indices for three selected time intervals (photometry presented in the Appendix, van Genderen et al. 2003b and Allen et al. 2005). Apart from the short-term oscillation, no binary-related cycle is visible in $U-B$. All cycles differ from each other. The coincidence of two peaks with the 1981.3 and 2003.5 PPs must be considered accidental, because their heights are not significantly different from the other ones (including the ones not shown in Fig. 14). Besides, no $U-B$ peak was present during the 1986.8 PP. During the 1975.8 PP, $U-B$ even showed a minimum, but it must be admitted that W-B probably did not show a peak as well, but the observations were poor. The 1992.4 and 1997.9 PPs coincided with gaps in the $U-B$ curve We wondered whether the phase-locked variable UV emission shown by the 2003 HST images (the 'Purple Haze') and emitted by gas lying at a considerable distance from the centre and also situated in the equatorial plane (Smith et al. 2004), was strong enough in the eighties to be responsible for the observed UV cycles in $W-B$. As since 2003 only U (UBV) observations were made, we have no indication about a possible excess-Balmer continuum radiation peak during the 2003.5 event. In order to explain the steep decline of the light peak in Johnson U and $U-B$ after the 2003.5 PP (Fig. 10), we suggested that this might be due to an UV deficit from the Purple Haze, arriving at the Earth weeks later than the actual moment that the UV shadow of the primary touches the ionized material far away in the equatorial plane (van Genderen & Sterken 2005). As numerous cycles of this kind occur all the time, we now conclude that the effect of the Purple Haze on the UBV photometry is very small.

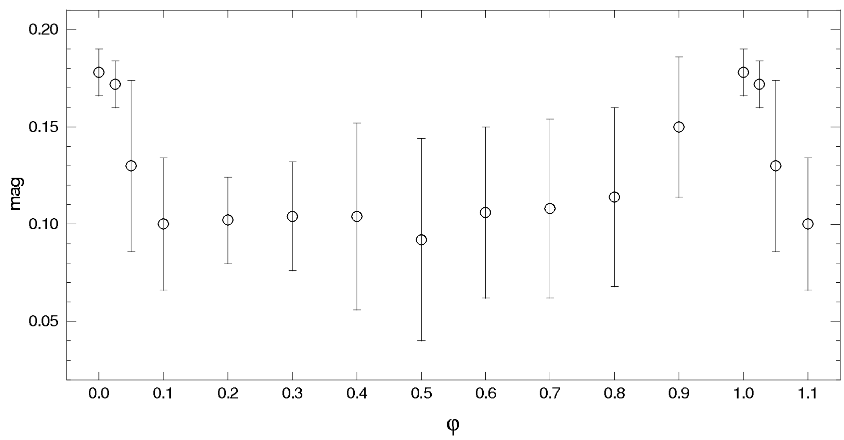

Figure 15: Mean *excess Balmer-continuum radiation* phase diagram with standard errors σ.

We noticed that an average from the excess-Balmer continuum curves in Fig. 8 in van Genderen et al. (1999) for the time interval 1978–1998 looks more or less similar to the X-ray light curve (Corcoran 2005). Fig. 15 shows this curve binned each 0.1 of the period (with the exception of the very steep descending branch where smaller steps were made). Bars are standard errors σ.

Like in the X-ray curve (Corcoran 2005), the steep descending branch is followed by a rather flat minimum, which eventually rises at a lower rate than the decline, until the maximum is reached near phase zero. We wondered whether equatorial gas close to, or inside the orbit, was ionized by the shocked wind of the primary, as the X-ray radiation of the colliding winds might be too weak to create enough ionizing photons, but this needs to be calculated (Corcoran 2005, private communication).

The relative large cycle-to-cycle variations in $W-B$, see the error bars in Fig. 15, and the absence of the phase-locked binary period in $W-B$ during a number of PPs, indicate that physical conditions in the gaseous environment of the binary strongly vary from cycle to cycle.

5.8.2 The 'few-100 d' oscillation

Fig. 14 shows no clear trend in the average Johnson $U-B$ value (-0.35) in the interval 1971.2–2006, nor any relationship with the PPs. This oscillation is not present in the adjacent medium broadbands at longer wavelengths and, therefore, we assume that this is due to the Balmer continuum radiation. The time scale for the oscillations hovers between 200^{d} and 400^{d}.

Thus, the periodicity of 200^{d}, extracted from the data 1992–1998, appears to be accidental, and consequently the tentative conclusions on the position of the periastron and the possible presence of a second companion have to be abandoned (van Genderen et al. 1999, 2001).

Its pseudo-periodicity rules out that emission lines of nebular knots are responsible for these oscillations. The Balmer continuum radiation from a star mainly originates in deep dense layers in the wind, e.g. deeper than the H emission lines, because it has a lower absorption coefficient. It is possible that stellar cyclic oscillations rule in some way the intensity of this Balmer continuum radiation and its outward transport. After all, it is quite normal that S Dor variables, such like R 127, R 40, P Cyg, etc., are subject to a number of different types of oscillations, some of which have time scales of a few hundred days (e.g. Sterken et al. 2001a; van Genderen et al. 1997; van Genderen et al. 2003c; de Groot et al. 2001; de Jager 2001; Markova et al. 2001a, b).

However, so far no other well-observed S Dor variable (LBV) has been found with the same type of Balmer continuum oscillation, but no other S Dor variable is known with such an extreme outer structure by the high rotation and with such an extreme wind as η Car (van Boekel et al. 2003).

6 Conclusions

i) We described the optical and near-infrared photometric features, light peak, dip and egress, during seven PPs of η Carinae. The size of peaks and dips seems to be independent of the gradual brightening of the Homunculus, suggesting that their cause is relatively stable. The same holds for the brightness of the primary, for which there is no indication for a change in luminosity over the last 35 year. Peaks are not caused by a hot spot nor by a flare, but are more likely the climax of the expansion phase of the primary due to tidal forces. The light maximum following the egress (out of the dip) is presumably part of the fading peak (the egress-maximum). The dip is explained by obscuration by the polar wind of the primary when the secondary's emitting circumstellar structure is occulted. The long-lasting deficit of each post-PP L and K radiation is explained by the model of Soker (2006b) and Akashi et al. (2006) involving the temporary annihilation of the wind by the collapse of the colliding wind region onto the secondary.

ii) The wavelength dependency of the linear secular brightening 1952–1997.8 ($0\overset{m}{.}025$ per year in V) is different from those of the post-egress brightening episodes after 1997.9 (star and Homunculus) and 2003.5 (Homunculus), especially in the NIR, see (iii). All appear to be different from the ordinary long-term light oscillations, which often show the S Dor-type signature. The secular brightening in the optical, mainly coming from the Homunculus, is likely the result of a mix of an extinction decrease and of changing emitting and scattering properties of gas and dust clouds as a result of the increased illumination and heating by the core due to the density decrease. The rates of the secular brightening in the NIR measured during the last 35 yr runs linearly. This radiation mainly comes from the core and the rates are largest in JHK, suggesting that its source, mainly free-free emission, is growing faster than the radiation in other bands (Whitelock et al. 2004). If this assumption is correct, it would mean that the mass of the stellar wind envelope is growing linearly, thus, the mass loss rate per orbital cycle was, on the average, constant over at least the last 35 yr

iii) The wavelength dependency of the 1997.9 fast brightening of the central star is analyzed with the aid of ground-based NIR observations and space-based (HST) observations. The analysis suggests that the brightening should be caused by a decrease of excess-extinction in the line of sight showing an anomalous extinction law with $R \sim 5.3$. Such a local dust clearance in the shell in the vicinity of the core just in the line of sight, would thus leave the brightness of the Homunculus unaltered. This conjecture also explains why the space-based observations of the core showed an increasing brightening rate with the decreasing size of the apertures. A globally thinning of the dust shell around the core, likely adding to the observed brightening of the central star (see above), should have been responsible for the simultaneous brightening by $0\overset{m}{.}3$ (in V) of the Homunculus starting 3 months after the 1997.9 PP. The same process seems to have happened causing the $0\overset{m}{.}25$ brightening (in V) after the 2003.5 PP (until early 2006). Their optical brightening rates also suggest that $R \sim 5$, but this needs confirmation.

iv) We found more confirmation that the Homunculus imitates the *intrinsic* light variations of the core very well. The mimicry in the optical becomes doubful if e.g. the brightness increases by a global dust clearance close around the core as discussed in (iii). The explanation could be that, for example, gas and dust particles are more fiercely illuminated and heated, in contrast to the weak light and temperature variations of the primary, giving rise to changes in the physics of gas and dust clouds inside the Homunculus, resulting in a varied wavelength dependency of their radiating and scattering properties.

v) The mean binary-related UV continuum cyclicity looks like the X-ray light curve and suggests revolution modulated H-emission variation in the equatorial plane. The 'few-100^d cyclicity' in the Balmer continuum radiation and present since the monitoring started 35 yr ago, hovers between 200^d and 400^d and may be related to stellar pulsations of the primary.

Acknowledgements

CS acknowledges support from the Belgian Fund for Scientific Research (FWO) and from the "IAP P5/36" Interuniversity Attraction Poles Programme of the Belgian Federal Office for Scientific, Technical and Cultural Affairs. The authors are indebted to the referee Dr. Noam Soker, and also to Dr. Hilmar W. Duerbeck, for a critical reading of the manuscript.

References

Abraham Z., Falceta-Gonçalves D., Dominic T.P., et al. 2005, A&A 437, 977
Akashi, M., Soker, N. & Behar, E. 2006, ApJ 644, 451
Allen, W.H., van Genderen, A.M. & Sterken, C. 2005, IBVS 5601
Allen, D.A. 1989, MNRAS 241, 195
Balick, B. & Matt, S. 2001, ASP Conf. Ser. 242, 155
van Boekel, R., Kervella, P., Schöller, M., et al. 2003, A&A 410, L37
Chesneau, O., Min, M., Herbst, T., et al. 2005, A&A 435, 1043
Corcoran, M.F., 2003, IAUC 8160, 3
Corcoran, M.F., 2005, AJ 129, 2018
Corcoran, M.F., Ishibashi, K., Swank, J.H. & Petre, R. 2001, ApJ 547, 1034
Damineli, A. 1996, ApJ 460, L49
Damineli, A., Stahl, O., Kaufer, A., et al. 1998, A&AS 133, 299
Davidson, K. 1999, ASP Conf. Ser. 179, 304
Davidson, K., Ebbets, D., Weigelt, G., et al. 1995, AJ 109, 1784
Davidson, K., Gull, T.R., Humphreys, R.M., et al. 1999, AJ 118, 1777
Davidson, K., Martin, J., Humphreys, R.M., et al. 2005, AJ 129, 900
Dwarkadas, V.V. & Owocki, S.P. 2002, AJ 581, 1337
ESA, The Hipparcos and Tycho Catalogues 1997, ESA SP-1200
Falceta-Gonçalves, D., Jatenco-Pereira, V. & Abraham, Z. 2005, MNRAS 357, 895
Feast, M.W., Whitelock, P.A. & Marang, F. 2001, MNRAS 322, 741
Feinstein, A. 1967, Obs. 87, 287
Feinstein, A. & Marraco, H.G. 1974, A&A 30, 271
Gehrz, R.D. & Smith, N. 1999, ASP Conf. Ser. 179, 251
van Genderen, A.M. 2001, A&A 366, 508
van Genderen, A.M. & Sterken C. 2004, A&A 423, L1

van Genderen, A.M. & Sterken, C., 2005, ASP Conf. Ser. 335, 343
van Genderen, A.M. & Thé, P.S. 1984, Space Sc. Rev. 39, 317
van Genderen, A.M., de Groot, M. & Thé, P.S. 1994, A&A 283, 89
van Genderen, A.M., de Groot, M. & Sterken, C. 1997, A&AS 124, 517
van Genderen, A.M., de Groot, M. & Sterken, C. 2001, ASP Conf. Ser. 233, 55
van Genderen, A.M., Sterken, C. & Allen, W.H. 2003a, A&A 412, L25
van Genderen, A.M., Sterken, C., Allen, W.H. & Liller, W. 2003b, A&A 405, 1057
van Genderen, A.M., Sterken, C. & de Groot, M. 2003c, Festschrift C. de Jager: Stars with Extended Atmospheres, Sterken C. (ed), University of Brussels, p.73
van Genderen, A.M., Sterken, C., de Groot, M. & Burki G. 1999, A&A 343, 847
van Genderen, A.M., Sterken, C., de Groot, M., et al. 1995, A&A 304, 415
Groh, J.H. & Damineli, A., 2004, IBVS 5492
de Groot, M., Sterken, C. & van Genderen, A.M. 2001, A&A 376, 224
Gull, T.R. & Ishibashi, K. 2001, ASP Conf. Ser. 242, 59
Gull, T.R., Ishibashi, K., Davidson, K. & Collins, N. 2001, ASP Conf. Ser. 242, 391
Hartman, H., et al. 2005, A&A 436, 945
Hillier, D.J. & Allen, D.A. 1992, A&A 262, 153
Hillier, D.J., Davidson, K., Ishibashi, K. & Gull, T. 2001, ApJ 553, 837
Iping, R.C., Sonneborn, G., Gull, T.R., et al. 2001, ASP Conf. Ser. 242, 55
Iping, R.C., Sonneborn, G., Gull, T.R., et al. 2005 ApJ 633, L37
Ishibashi, K., Corcoran, M., Davidson, K., et al. 1999, ApJ 524, 983
de Jager, C., 2001, ASP Conf. Ser. 233, 215
King, N.L., Nota, A., Walsh, J.R., et al. 2002, ApJ 581, 285
Lajús, F.E., Gamen, R., Schwartz, M., et al. 2003, IBVS 5477
Markova, N., Scuderi, S., de Groot, M., et al. 2001a, A&A 366, 935
Markova, N., Morris, N., Kolka, I. & Markov, H. 2001b, A&A 376, 898
Martin, J.C. & Koppelman, M.D., HST Treasury team 2004, AJ 127, 2352
Niemela, V., Lajús, E.F., Schwartz, M., et al. 2005, La Plata Website 11 October 2005
Pittard, J.M. & Corcoran, M.F. 2002, A&A 383, 636
Robinson, G., Mitchell, R.M., Aitken, D.K., et al. 1987, MNRAS 227, 535
Soker, N. 2000, MNRAS 312, 217
Soker, N. 2003, ApJ 597, 513
Soker, N. 2004, ApJ 612, 1060
Soker, N. 2005a, ApJ 619, 1064
Soker, N. 2005b, ApJ 635, 540
Savage, B.D. & Mathis, J.S. 1979, Ann. Rev. Astron. Astroph. 17, 73
Smith, N. & Gehrz, R.D. 2000, ApJ 529, L99
Smith, N., Gehrz, R.D., Hinz, P.M., et al. 2003a, AJ 125, 1458
Smith, N., Morse, J.A., Collins, N.R. & Gull T.R. 2004, ApJ 610, L105
Smith, N., Morse, J., Davidson, K. & Humphreys, R.M. 2000, AJ 120, 920

Smith, N., Davidson, K., Gull, T.R., et al. 2003b, ApJ 586, 432

Stahl, O., Weis, K., Bomans, D.J., et al. 2005, A&A 435, 303

Steenman, H. & Thé, P.S. 1989, Astrophys. Sp. Sc. 189, Kluwer, Dordrecht, p.189

Steiner, J.E. & Damineli, A. 2004, ApJ 612, L133

Sterken, C., van Genderen, A.M., de Groot, M. & Burki G. 1999a, ASP Conf. Ser. 179, 200

Sterken, C., Freyhammer, L., Arentoft, T. & van Genderen, A.M. 1999b, A&A 346, L33

Sterken, C., Freyhammer, L., Arentoft, T., et al. 2001a, ASP Conf. Ser. 233, 71

Sterken, C., Freyhammer, L., Arentoft, T., et al. 2001b, in A Decade of HST Science, Livio M., Noll K., (eds), p.89

Sterken, C., et al. 2006, in preparation

Verner, E.M., Gull, T.R., Bruhweiler, F., et al. 2002, ApJ 581, 1154

Viotti, R., Corcoran, M., Damineli, A., et al. 1998, in Ultraviolet Astrophysics Beyond the IUE Final Archive, Harris R.A. (ed), ESA SP-1200, p.297

Viotti, R. & Rossi, C. 1999, ASP Conf. Ser. 179, 211

Walsh, J.R. & Ageorges, N. 2000, A&A 357, 255

Whitelock, P.A. & Laney, C. 1999, ASP Conf. Ser. 179, 258

Whitelock, P.A., Feast, M.W., Koen, C., et al. 1994, MNRAS 270, 364

Whitelock, P.A., Feast, M.W., Marang, F. & Breedt E. 2004, MNRAS 352, 447

Appendix: the new optical photometric observations

The 1972–2002 Auckland data set

Until 1990 the telescope used was the 50-cm Edith Winstone Blackwell telescope (f 13.3 Cassegrain) at Auckland Observatory, with an EMI 9502 tube. After 1990 the Harry Williams 53-cm reflector with an EMI 9924 tube was used. The observervations were made by one of us (WSGW).

The aperture used was 31 arcsec at Auckland Observatory, and a 60-arcsec aperture was used at Milton Road. After 1990 the tube was replaced by an EMI 9924 tube. The comparison star was HD 93695 (B5 V), $V = 6.47$, $B-V = -0.13$ (Cousins & Stoy 1963), $U-B = -0.600$ as transformed from the $(U-B)c$ given in the latter reference. It appeared that it is suspected as a weak variable star (NSV 4978, Kukarkin et al. 1982). The Hipparcos catalogue (ESA 1997) reports a spread of $0\overset{\text{m}}{.}007$ only. Considering the spread in the light and colour curves, the variations were indeed small. The star HD 93131 (WN, $V = 6.48$, $B-V = -0.03$, $U-B = -0.89$, Mermilliod & Mermilliod 1994) served as a check star. The sky measurements were always taken at the same spot midway between HD 93695 and HD 93737. From 1994 until 2002 the observations were continued at the Milton Road Observatory, close to the Auckland Observatory, with a 50-cm reflector and a 60 arcsec aperture. All data are listed in Table 4.

The 2002–2005 Blenheim data set

In a previous paper (van Genderen et al. 2003a), we have discussed the UBV photometry made by one of us (WHA) around the 1992.4 PP. Despite the rather limited stability of the photometer at the time – especially in the U channel – the data were useful for identifying the optical event. Moreover, the U magnitudes were too bright by $0\overset{\text{m}}{.}3$ on the average (van Genderen et al. 2003b; Allen et al. 2005). At last the problem was solved and we present here the improved photometry with photometric parameters of the two comparison stars[5]. Star A = HD 93010 is a visual binary (but both stars were measured): $V = 6.390$, $B-V = 0.000$ (Cousins & Stoy 1963), $U-B = -0.560$. This value is given by Feinstein (1967) and only refers to the brightest component of the binary. As the other component is fainter and is of the same spectral type, we adopted the same $U-B$ value for both. Star B = HD 93502: $V = 6.250$, $B-V = 0.040$, $U-B = 0.040$ (taken from the catalogue of Mermilliod & Mermilliod 1994, listing averages from various sources). All data are listed in Table 5, including data not plotted in Fig. 14.

References for Appendix

Allen, W.H., van Genderen, A.M. & Sterken, C. 2005, IBVS 5601

Cousins, A.W.J. & Stoy, R.H. 1963, Roy. Obs. Bull. no.64

ESA, The Hipparcos and Tycho Catalogues 1997, ESA SP-1200

Feinstein, A. 1967, Obs. 87, 287

Kukarkin, B.V., Kholopov P.N., Artiukhina N.M., et al. 1982, New General Catalogue of Suspected Variable Stars, Nauka, Moscow

Mermilliod, J.C. & Mermilliod M. 1994, Catalogue of Mean UBV Data on Stars, Springer Verlag

van Genderen, A.M., Sterken C. & Allen W.H. 2003a, A&A 405, 1057

van Genderen, A.M., Sterken, C., Allen, W.H. & Liller, W. 2003b, A&A 412, L25

[5]For data from JD 2452506 onwards. Magnitudes and colours before that date are less reliable: ±0.1 in V, ±0.05 in $B-V$, and ±0.3 in $U-B$.

Table 4: *UBV* photometry, the Auckland set.

JD	V	B − V	U − B	JD	V	B − V	U − B
41033.97	6.01	0.58	−0.36	42201.14	6.11	0.64	
41034.91	6.01	0.59	−0.35	42201.77	6.13	0.61	−0.37
41037.11	6.03	0.60	−0.33	42218.77	6.15	0.61	−0.37
41067.05	6.00	0.60	−0.35	42233.86	6.13	0.63	−0.36
41069.87	6.00	0.61	−0.37	42593.79	6.04	0.60	−0.37
41078.91	6.01	0.61	−0.37	42597.87	6.02	0.62	−0.35
41097.76	5.97	0.60	−0.37	42599.78	6.04	0.63	−0.38
41119.78	5.96	0.61	−0.36	42624.79	6.00	0.63	−0.38
41123.76	5.97	0.61	−0.38	42627.79	6.01	0.62	−0.34
41129.80	5.94	0.61	−0.37	42635.80	6.00	0.62	−0.34
41132.77	5.95	0.62	−0.36	42640.78	6.07	0.60	−0.37
41136.79	5.96	0.60	−0.33	42668.80	5.98	0.64	−0.32
41139.84	5.97	0.57	−0.34	42731.04	5.96	0.60	−0.35
41145.77	5.96	0.59	−0.35	42809.94	5.93	0.59	−0.34
41147.78	5.97	0.58	−0.34	42831.94	5.93	0.61	−0.38
41148.83	5.97	0.59	−0.33	42835.89	5.90	0.61	−0.38
41150.77	5.96	0.61	−0.35	42837.02	5.90	0.61	−0.38
41155.83	5.97	0.61	−0.33	42855.03	5.94	0.67	−0.33
41169.81	5.96	0.60	−0.32	42855.92	5.89	0.61	−0.39
41172.87	5.96	0.62		43370.82	6.06	0.57	−0.33
41180.79	6.00	0.61	−0.33	43436.07	6.04	0.57	−0.32
41182.80	5.96	0.58	−0.32	43545.05	6.02	0.58	−0.37
41197.80	5.95	0.58	−0.32	43549.92	6.01	0.59	−0.38
41209.80	5.99	0.64	−0.32	43564.01	6.02	0.60	−0.38
41258.09	5.97	0.61	−0.35	43590.04	6.03	0.57	−0.36
41268.06	6.03	0.61	−0.35	43605.81	6.07	0.57	−0.37
41290.96	6.04	0.59	−0.33	43608.82	6.03	0.59	−0.38
41341.94	6.03	0.58	−0.38	43620.91	6.00	0.63	−0.38
41348.94	6.04	0.61	−0.35	43621.92	6.05	0.60	−0.39
41349.97	6.07	0.60	−0.41	43624.95	6.04	0.59	−0.39
41350.96	6.04	0.60	−0.38	43647.82	6.03	-	-
41480.76	6.04	0.61	−0.37	43656.83	6.05	0.58	−0.39
41484.78	6.04	0.61	−0.37	43662.90	5.99	0.57	−0.36
41496.91	6.03	0.63	−0.36	43690.86	6.04	0.58	−0.38
41729.95	6.08	0.58	−0.36	43704.82	5.99	0.59	−0.37
41777.00	6.05	0.61	−0.36	43705.86	5.99	0.61	−0.36
41779.05	6.09	0.60	−0.34	43725.83	6.01	0.60	−0.37
41828.79	6.07	0.61	−0.36	43890.87	5.93	0.58	−0.33
41862.87	6.06	0.61	−0.36	43914.91	5.94	0.60	−0.39
41863.88	6.02	0.60	−0.34	43958.82	5.95	0.60	−0.39
41865.81	6.08	0.61	−0.37	44033.81	5.99	0.62	−0.40
41866.78	6.11	0.61	−0.36	44062.85	5.93	0.62	−0.37
41870.79	6.09	0.63	−0.38	44090.82	5.93	0.61	−0.36
41882.80	6.07	0.58	−0.35	44208.96	5.94	0.61	−0.34
41890.78	6.09	0.59	−0.34	44215.97	5.92	0.61	−0.34
42061.87	6.00	0.59	−0.36	44223.96	5.92	0.60	−0.35
42071.95	6.02	0.58	−0.39	44228.90	5.92	0.61	−0.33
42072.87	6.05	0.60	−0.34	44311.91	5.97	0.60	−0.34
42075.88	6.10	0.56	−0.43	44343.97	5.97	0.59	−0.36
42080.06	6.02	0.59	−0.37	44348.88	5.96	0.61	−0.37
42084.92	5.99	0.61	−0.38	44367.89	5.95	0.58	−0.36
42103.91	5.99	0.62	−0.40	44369.81	5.97	0.59	−0.36
42162.11	6.10	0.64		44397.88	5.94	0.59	−0.36
42162.84	6.08	0.61	−0.39	44398.86	5.94	0.59	−0.37
42164.02	6.06	0.62	−0.36	44418.84	5.94	0.59	−0.36
42166.08	6.09	0.63	−0.33	44444.83	5.94	0.60	−0.34
42166.83	6.06	0.59	−0.37	44461.80	5.96	0.55	−0.33
42173.88	6.08	0.60	−0.40	44482.81	5.92	0.63	−0.32
42183.91	6.05	0.62	−0.39	44525.85	5.94	0.56	–
42197.90	6.19	0.62	−0.34	44535.96	5.90	0.64	–

Table 4: *UBV* photometry, the Auckland set (continued).

JD	V	$B-V$	$U-B$	JD	V	$B-V$	$U-B$
44579.99	5.88	0.58	−0.36	46847.85	5.80	0.62	−0.38
44609.95	5.86	0.59	−0.39	46924.94	5.80	0.58	−0.36
44674.95	5.85	0.61	−0.41	46953.88	5.82	0.58	−0.37
44677.95	5.83	0.62	−0.41	47512.97	5.815	0.56	−0.41
44691.97	5.79	0.61	−0.41	48051.90	5.76	0.54	−0.41
44692.94	5.79	0.61	−0.40	49031.04	5.63	0.59	−0.44
44694.97	5.80	0.62	−0.40	49054.95	5.61	0.59	−0.43
44698.88	5.80	0.59	−0.41	49094.98	5.56	0.59	−0.36
44702.86	5.807	0.608	−0.41	49100.94	5.59		
44710.82	5.77	0.63	−0.44	49108.94	5.56	0.59	−0.43
44713.97	5.759	0.622	−0.42	49371.89	5.52	0.65	−0.28
44718.97	5.75	0.63	−0.43	49414.87	5.58	0.64	−0.27
44724.85	5.73	0.63	−0.44	49509.83	5.63	0.59	−0.40
44725.96	5.739	0.618	−0.43	49510.93	5.63	0.61	−0.38
44727.82	5.742	0.620	−0.41	49715.97	5.64	0.59	−0.32
44734.82	5.698	0.605	−0.43	49730.95	5.64	0.61	−0.23
44735.87	5.703	0.603	−0.44	49746.96	5.67	−	−
44746.90	5.782	0.617	−0.41	49794.98	5.70	0.62	−0.44
44747.88	5.79	0.62	−0.41	49801.04	5.70	0.61	−0.42
44748.79	5.79	0.62	−0.42	49803.03	5.74	0.64	−0.42
44752.85	5.800	0.611	−0.40	50847.95	5.44	0.64	−0.28
44760.84	5.79	0.64	−0.40	50850.94	5.41	0.65	−0.28
44766.82	5.79	0.63	−0.41	50856.93	5.42	0.67	−0.27
44776.82	5.797	0.652	−0.38	51319.84	5.22	0.66	−0.31
44780.83	5.78	0.66	−0.38	51620.87	5.10	0.67	−0.30
44786.76	5.78	0.65	−0.39	51625.92	5.10	0.67	−0.33
44797.99	5.78	0.65	−0.38	51627.85	5.09	0.70	−0.30
44805.81	5.77	0.65	−0.38	51630.87	5.10	0.67	−0.31
44982.93	5.74	0.590	−0.34	51635.89	5.10	0.68	−0.32
44986.00	5.76	0.600	−0.36	51666.93	5.11	0.67	−0.31
45001.33	5.78	0.58	−0.35	51688.82	5.12	0.65	−0.38
45048.04	5.75	0.600	−0.35	51703.86	5.17	0.68	−0.30
45056.90	5.75	0.61	−0.37	51710.84	5.18	0.67	−0.30
45138.98	5.77	0.620	−0.32	51725.03	5.17	0.71	−0.26
45159.88	5.79	0.60	−0.33	52302.88	5.14	0.72	−0.32
45360.87	5.80	0.60	−0.37	52307.96	5.16	0.70	−0.33
45403.84	5.82	0.600	−0.39	52322.94	5.14	0.67	−0.30
45505.91	5.86	0.58	−0.39	52322.94	5.14	0.70	−0.33
45520.76	5.88	0.61	−0.41	53612.81	4.969	0.604	−0.36
45533.77	5.88	0.59	−0.39	53658.02	4.931	0.575	−0.35
45574.79	5.92	0.58	−0.34	53678.06	4.908	0.593	−0.43
45667.91	5.86		−0.38	53410.89	4.944	0.623	−0.43
45720.89	5.94	0.57	−0.40	53420.07	4.954	0.616	−0.46
45749.86	5.95	0.56	−0.42	53423.86	4.977	0.589	−0.45
45775.92	5.94	0.55	−0.41	53465.87	4.994	0.608	−0.46
45876.87	5.94	0.55	−0.40	53481.85	5.007	0.609	−0.45
45944.82	5.88	0.60	−0.40	53499.86	4.995	0.614	−0.46
46218.88	5.89	0.57	−0.43	53511.78	5.016	0.581	−0.52
46695.81	5.80	0.57	−0.28	53511.83	5.004	0.564	−0.50
46699.82	5.76	0.59	−0.23	53553.91	4.998	0.603	−0.40
46805.94	5.79	0.60	−0.36	53587.84	5.034	0.591	−0.39
46806.90	5.80	0.61	−0.34				

Table 5: UBV photometry, the Blenheim set.

JD	V	$B-V$	$U-B$	JD	V	$B-V$	$U-B$
48059.940	5.68	0.61	−0.44	51606.8692	5.12	0.70	−0.33
48062.870	5.61	0.65	−0.45	51612.8989	5.13	0.67	−0.29
48070.890	5.65	0.63	−0.41	52506.920	5.324	0.634	−0.264
48269.080	5.68	0.64	−0.44	52509.228	5.277	0.526	−0.313
48282.920	5.68	0.66	−0.38	52509.833	5.301	0.537	−0.372
48378.850	5.63	0.64	−0.47	52515.829	5.282	0.541	−0.384
48378.850	5.63	0.64	−0.47	52638.853	5.298	0.53	−0.272
48385.880	5.64	0.64	−0.46	52647.121	5.252	0.612	−0.444
48386.840	5.64	0.64	−0.45	52654.960	5.271	0.601	−0.424
48390.830	5.61	0.63	−0.45	52678.911	5.317	0.589	−0.446
48391.990	5.59	0.64	−0.42	52695.876	5.248	0.611	−0.428
48705.933	5.68	0.73	−0.33	52700.876	5.26	0.612	−0.434
48711.889	5.67	0.76	−0.28	52700.946	5.26	0.611	−0.441
48719.885	5.65	0.75	−0.29	52703.141	5.221	0.61	−0.434
48728.837	5.63	0.80	−0.22	52703.181	5.233	0.617	−0.418
48763.863	5.46	0.76	−0.86	52717.831	5.224	0.614	−0.427
48775.830	5.43	0.78	−0.88	52717.898	5.228	0.618	–
48775.915	5.53	0.80	−0.76	52722.844	5.23	0.613	−0.444
48794.808	5.39	0.77	−0.81	52732.839	5.199	0.626	−0.443
48797.824	5.52	0.76	−0.80	52744.802	5.186	0.629	−0.452
48998.0277	5.59	0.57	−0.37	52746.852	5.198	0.624	−0.459
49025.891	5.66	0.64	−0.47	52749.922	5.194	0.62	−0.449
49026.891	5.67	0.66	−0.40	52754.808	5.185	0.63	−0.454
49029.945	5.67	0.64	−0.46	52754.907	5.208	0.623	−0.463
49031.0401	5.63	0.59	−0.44	52755.791	5.175	0.63	−0.453
49054.9586	5.61	0.59	−0.43	52762.783	5.168	0.627	−0.463
49060.858	5.63	0.61	−0.58	52771.846	5.153	0.638	−0.451
49100.9497	5.59	–	–	52772.781	5.152	0.638	−0.449
49108.9431	5.56	0.59	−0.43	52772.840	5.155	0.640	−0.453
49371.8952	5.52	0.65	−0.28	52786.947	5.152	0.626	−0.439
49414.8765	5.58	0.64	−0.27	52787.875	5.152	0.628	−0.462
49509.8312	5.63	0.59	−0.40	52788.891	5.152	0.624	−0.476
49510.9388	5.63	0.61	−0.38	52789.940	5.158	0.636	−0.451
49715.9780	5.64	0.59	−0.32	52790.903	5.120	0.627	−0.457
49730.9590	5.64	0.61	–	52797.841	5.119	0.643	−0.463
49746.9603	5.67	–	–	52800.892	5.091	0.639	−0.441
49794.9859	5.70	0.62	−0.44	52806.777	5.096	0.645	−0.477
49801.0461	5.70	0.61	−0.42	52813.836	5.062	0.634	−0.452
49803.0399	5.74	0.64	−0.42	52814.823	5.07	0.639	−0.465
50847.9544	5.44	0.64	−0.28	52814.836	5.06	0.636	−0.452
50850.9404	5.41	0.65	−0.28	52815.806	5.06	0.639	−0.466
50856.9378	5.42	0.67	−0.27	52817.863	5.054	0.636	−0.438
51319.8457	5.22	0.66	−0.31	52817.841	5.06	0.633	−0.443
51322.8565	5.18	0.67	−0.32	52821.771	5.047	0.632	−0.452
51335.8660	5.22	0.67	−0.33	52822.863	5.058	0.626	−0.434
51336.8543	5.22	0.65	−0.32	52833.778	5.141	0.630	−0.400
51348.8614	5.22	0.68	−0.29	52833.832	5.140	0.632	−0.383
51349.8440	5.18	0.67	−0.29	52835.847	5.108	0.694	−0.355
51560.9347	5.13	0.68	−0.29	52837.776	5.150	0.633	−0.384
51560.9347	5.13	0.70	−0.30	52838.781	5.147	0.638	−0.378
51606.8692	5.12	0.67	−0.32	52856.226	5.112	0.630	–

Table 5: UBV photometry, the Blenheim set (continued).

JD	V	$B-V$	$U-B$	JD	V	$B-V$	$U-B$
52856.790	5.101	0.653	−0.351	53420.076	4.954	0.616	−0.460
52861.824	5.083	0.651	−0.330	53423.860	4.977	0.589	−0.452
52867.801	5.065	0.653	−0.339	53465.876	4.994	0.608	−0.463
52870.807	5.070	0.647	−0.338	53481.858	5.007	0.609	−0.456
52876.851	5.071	0.649	–	53499.861	4.995	0.614	−0.461
52884.799	5.088	0.641	−0.311	53511.788	5.016	0.581	−0.529
53004.911	5.074	0.607	−0.331	53511.831	5.004	0.564	−0.507
53095.831	5.058	0.626	−0.414	53553.911	4.998	0.603	−0.406
53109.003	5.10	0.622	−0.419	53587.847	5.034	0.591	−0.394
53151.897	5.046	0.624	−0.428	53612.813	4.969	0.604	−0.360
53163.775	5.043	0.635	−0.443	53658.026	4.931	0.575	−0.351
53238.839	5.044	0.599	−0.334	53678.067	4.908	0.593	−0.434
53239.163	5.044	0.609	−0.296	53724.926	4.889	0.611	−0.403
53266.811	4.999	0.611	−0.286	53726.106	4.871	0.619	−0.445
53304.985	5.020	0.607	−0.332	53755.953	4.833	0.619	−0.420
53318.058	4.965	0.601	−0.313	53785.917	4.816	0.618	−0.427
53334.871	4.954	0.615	−0.311	53960.810	4.802	0.605	–
53338.875	4.959	0.582	−0.283	53963.818	4.942	0.606	−0.405
53345.897	5.012	0.588	−0.382	53990.835	4.869	0.600	–
53349.947	4.986	0.592	−0.420	53992.199	4.867	0.584	−0.486
53377.096	4.994	0.609	−0.456	54034.119	4.885	0.596	−0.397
53396.894	4.95	0.614	−0.419	54048.008	4.918	0.586	−0.356
53410.890	4.944	0.623	−0.435				